Chapter 3

Observations

3.1 INTRODUCTION

In the late 1950s, a ground-based tracking system known as *Minitrack* was installed to track the Vanguard satellites. This system, which was based on radio interferometry, provided a single set of angle observations when the satellite passed above an instrumented station's horizon. These angle measurements, collected from a global network of stations over several years, were used to show that the Earth had a pear-shape. They also provided the means to investigate the nature of forces acting on Vanguard and their role in the multiyear orbit evolution of the satellite.

A variety of observations are now available to support the determination of a satellite orbit. For the most part, these observations are collected by instrumentation that measures some scalar quantity related to the satellite's position or velocity. Modern systems such as the *Global Positioning System* (GPS) provide the position of a GPS receiver, but even GPS requires the use of scalar measurements to determine the orbits of the individual satellites that comprise the GPS constellation. The dependence of scalar measurements on the satellite state (position and velocity) is a key element in the orbit determination process.

Section 3.2 describes an ideal representation of the commonly used measurements. This ideal representation not only serves as an introduction to the measurement type, it also can be used for simulations and other analyses of the orbit determination process. A more realistic description of those measurements is provided in Section 3.3, but from a conceptual viewpoint. The hardware realization of the measurements is discussed in Section 3.4, including other effects, such as those associated with propagation of signals through the atmosphere. The hardware realization must be modeled in terms of the orbit parameters to be determined; hence, this modeling produces a *computed observation*, which is an

essential part of the orbit determination process. Examples of measurements obtained by selected instrumentation are discussed in Section 3.5. The use of differenced measurements to remove errors with specific characteristics is discussed in Section 3.6. The use of a satellite ephemeris and angles are discussed in the final sections of this chapter. Supplementary material can be found in Montenbruck and Gill (2001) and Seeber (1993).

3.2 OBSERVATIONS

3.2.1 IDEAL RANGE

A common measurement in orbit determination is the distance between an Earth-based instrument performing the measurement and the satellite. If the position vector of an instrument is $\mathbf{r}_I$ and the position vector of the satellite is $\mathbf{r}$, the ideal range ρ is the scalar magnitude of the position vector of the satellite with respect to the instrument,

$$\rho = [(\mathbf{r} - \mathbf{r}_I) \cdot (\mathbf{r} - \mathbf{r}_I)]^{1/2}. \tag{3.2.1}$$

In this ideal representation, the range should be more precisely described as the *geometric range* or *instantaneous range*, since it represents the instantaneous, geometric distance between the measuring instrument and the satellite. This ideal representation has ignored subtle issues, such as the finite speed of light and the fact that ρ is the distance between a specific point within the instrument and a specific point on the satellite. Furthermore, if ρ_{obs} represents the measured range at time t, $\mathbf{r}$ and $\mathbf{r}_I$ represent the true position vectors at this time, then ρ and ρ_{obs} are related by

$$\rho_{\text{obs}} = \rho + \epsilon \tag{3.2.2}$$

where ϵ represents instrumental errors and propagation delays. Note also that if the position vectors $\mathbf{r}$ and $\mathbf{r}_I$ are in error, then ϵ must contain terms that would be necessary to make Eq. (3.2.2) an equality.

The geometric range, ρ, is invariant under rotation of axes used to describe $\mathbf{r}$ and $\mathbf{r}_I$. That is, if (X, Y, Z) represents an inertial system and (x, y, z) represents an Earth-fixed system, the geometric range can be expressed as

$$\rho = [(X - X_I)^2 + (Y - Y_I)^2 + (Z - Z_I)^2]^{1/2} \tag{3.2.3}$$

or

$$\rho = [(x - x_I)^2 + (y - y_I)^2 + (z - z_I)^2]^{1/2} \tag{3.2.4}$$

where ρ is identical for both representations.

3.2.2 IDEAL RANGE RATE

In some cases, the time rate of change of the range, or range-rate, may be the measured quantity. From the expression of range in the (X, Y, Z) nonrotating system, Eq. (3.2.3), differentiation with respect to time yields

$$\begin{aligned}\dot{\rho} &= \Big[(X - X_I)(\dot{X} - \dot{X}_I) + (Y - Y_I)(\dot{Y} - \dot{Y}_I) \\ &\quad + (Z - Z_I)(\dot{Z} - \dot{Z}_I)\Big] \Big/ \rho \end{aligned} \tag{3.2.5}$$

or

$$\dot{\rho} = \frac{\boldsymbol{\rho} \cdot \dot{\boldsymbol{\rho}}}{\rho} \tag{3.2.6}$$

where $\boldsymbol{\rho} = (X - X_I)\mathbf{u}_X + (Y - Y_I)\mathbf{u}_Y + (Z - Z_I)\mathbf{u}_Z$, the position vector of the satellite with respect to the instrument. The relative velocity is

$$\dot{\boldsymbol{\rho}} = (\dot{X} - \dot{X}_I)\mathbf{u}_X + (\dot{Y} - \dot{Y}_I)\mathbf{u}_Y + (\dot{Z} - \dot{Z}_I)\mathbf{u}_Z. \tag{3.2.7}$$

Note that the position and velocity of a ground-based instrument expressed in the nonrotating (X, Y, Z) system will be dependent on the rotation of the Earth.

Equation (3.2.6) can readily be interpreted as the component of the relative velocity in the direction defined by the relative position vector, $\boldsymbol{\rho}$. In other words, the range-rate is the component of the relative velocity between the observing instrument and the satellite in the line-of-sight direction—the direction defined by $\boldsymbol{\rho}$. As described in the preceding section, if $\dot{\rho}_{\text{obs}}$ is the observed parameter, then $\dot{\rho}_{\text{obs}}$ is equal to $\dot{\rho}$ plus the inclusion of instrumental, media, and other errors.

3.2.3 IDEAL AZIMUTH AND ELEVATION ANGLES

A topocentric system was defined in Section 2.4.3. If the relative position vector, $\boldsymbol{\rho}$, is expressed in this system, then the angles, azimuth and elevation, can be defined, as noted in Section 2.4.3. The angles are illustrated in Fig. 2.4.4.

3.2.4 EXAMPLES: IDEAL OBSERVATIONS

In Example 2.2.4.1, the initial conditions for a Shuttle-like orbit were given and the state was predicted forward in time with Example 2.2.5. This ephemeris was transformed into Earth-fixed coordinates and the ground track can be found in Fig. 2.2.7. If the initial conditions differ by 1 meter in the radial component with respect to those in Example 2.2.4.1, the difference between the two ephemerides is illustrated in Fig. 2.2.9 for about two orbital revolutions. If the "perturbed" initial conditions in Example 2.2.6.1 are assumed to represent the "truth," then a set of *simulated observations* can be generated. For this discussion, simulated

Table 3.2.1:
Coordinates of Simulated Ranging Instruments

	Earth-Fixed Coordinates			Geocentric	
Site	x (m)	y (m)	z (m)	Latitude	Longitude
FZ	4985447.872	−3955045.423	−428435.301	3.8516°S	38.4256°W
EI	−1886260.450	−5361224.413	−2894810.165	26.9919°S	109.3836°W

FZ: Fortaleza

EI: Easter Island

Note: x,y,z computed from latitude, longitude, and a spherical Earth with radius 6378137.0 m

observations are represented by geometric ranges (Section 3.2.1) and range-rate (Section 3.2.2). Simulated observations are useful to characterize different error sources in a controlled experiment.

Consider two hypothetical sites capable of making range measurements: Easter Island and Fortaleza, Brazil. Assume the true coordinates of these two sites are given in Table 3.2.1. The ground tracks of the orbit in the vicinity of these sites are illustrated in Fig. 3.2.1, extracted from the global ground tracks shown in Fig. 2.2.6. The interval while the satellite is above the station's horizon is termed a *pass*. In some cases, the measurements below a specified elevation may be ignored, usually referred to as the *elevation mask*. The first candidate pass from Fortaleza rises less than 1° in elevation, so with a 5° elevation mask, for example, this pass would be ignored. An elevation mask usually is adopted to edit low-elevation passes because of poor signal-to-noise ratios, excessive atmospheric refraction, or multipath effects. For the case shown in Fig. 3.2.1, two passes are observed from Easter Island and one pass from Fortaleza, ignoring the very low-elevation pass at Fortaleza.

The geometric ranges to the satellite observed by each station over three passes are shown in Fig. 3.2.2, where time is measured from the time of the initial state given in Example 2.2.4.1. The minimum range point in each plot is the *point of closest approach* of the satellite to the station. If the ranging instrument had a measurement noise at the one meter level, it is clear that this characteristic would not be visually obvious in Fig. 3.2.2.

The range-rates observed from Easter Island are shown in Fig. 3.2.3. Since range-rate is the time derivative of range, the point of minimum range corresponds to zero range-rate.

A *sky plot* is a useful way to visualize the geometry of a satellite pass above an

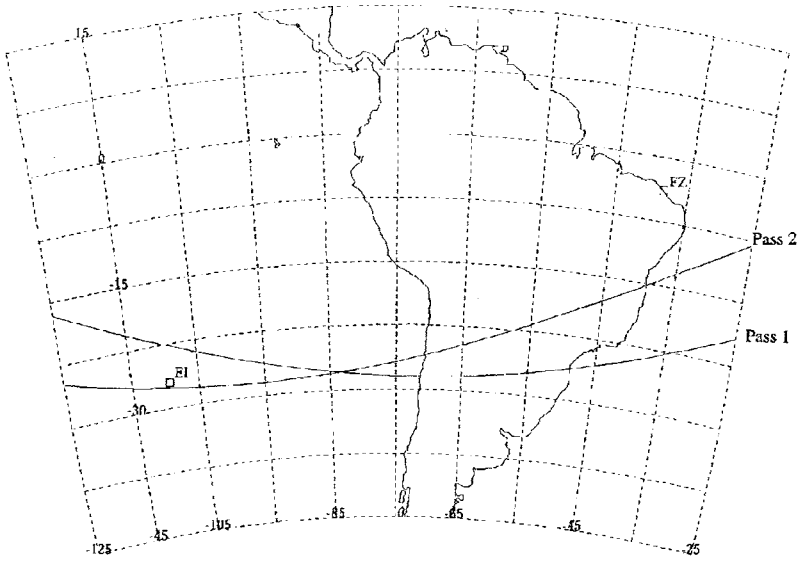

Figure 3.2.1: Portion of shuttle ground track from Fig. 2.2.6. The two orbital revolutions in the vicinity of simulated tracking stations at EI (Easter Island) and FZ (Fortaleza) produce two passes that are within view of the stations. However, the satellite in Pass 1 at Fortaleza rises above the horizon by less than 5° in elevation.

observing station's horizon. The sky plot for each of the three passes illustrated in Fig. 3.2.2 is shown in Fig. 3.2.4. The concentric circles represent an elevation increment of 30°, where the outermost circle is the station's horizon (0° elevation), and the center point is 90° elevation (directly overhead the station). The plot shows the azimuth, measured eastward from north. For example, for Pass 1 from Easter Island, the satellite rises above the station horizon at an azimuth of $-59°$ (i.e., 59° west of north) and sets at 96° azimuth (96° east of north). The highest elevation for this pass is about 40° at an azimuth of 23°.

If the initial conditions in Example 2.2.6.2 represent the true initial conditions, and the set given by Example 2.2.4.1 are used as a nominal or reference set, a *residual* can be formed as the *observed minus computed*, or *O minus C* ($O - C$). Within the context of orbit determination applications, the true initial conditions are unknown, but the observations represented by the ranges in Fig. 3.2.2 are the result of the true state and the measuring instrument characteristics. Usually, a nominal set of initial conditions are available but they deviate from the true values. Nevertheless, based on the nominal initial conditions, a *computed range* can be formed. The resulting residuals for the three passes are shown in Fig.

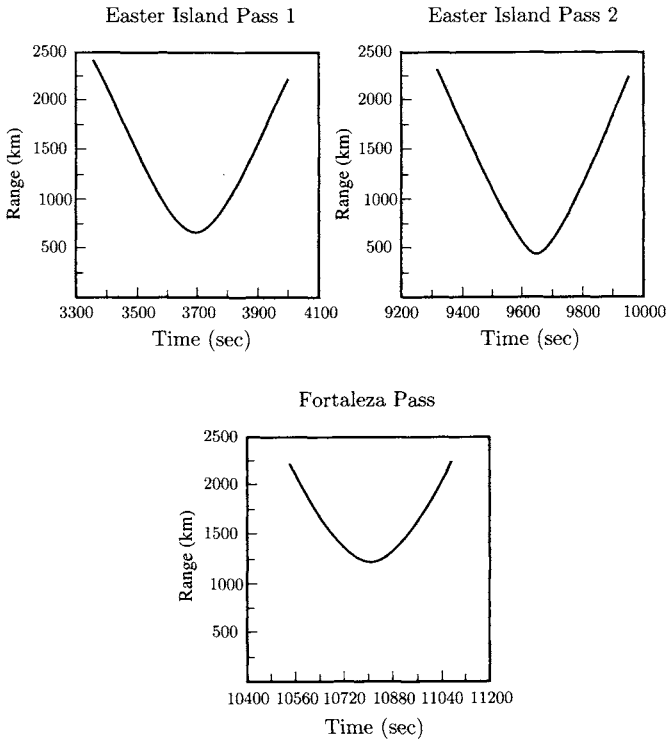

Figure 3.2.2: Simulated range vs time. These plots show the geometric range vs time measured by the two sites, Easter Island and Fortaleza, shown in Fig. 3.2.1.

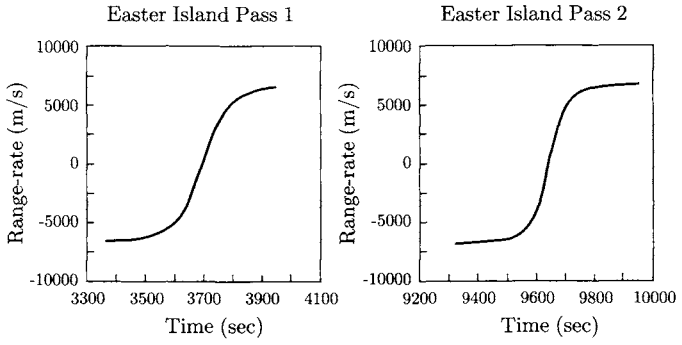

Figure 3.2.3: Simulated range-rate vs time.

3.2.5. It has been assumed that all ranges are instantaneous and no atmospheric delays have been included in these simulations. In essence, the residuals in Fig. 3.2.5 illustrate how the orbit differences of Fig. 2.2.9 are exhibited in terms of range residuals from ground-based stations.

Consider the residual, $O - C$, for the second pass from Easter Island. As shown in the sky plot for this pass in Fig. 3.2.4, the satellite passes nearly overhead, with a maximum elevation of about 78°. When the satellite rises above the Easter Island horizon in the west, the measured range reflects a significant component in the along-track direction. As described in Section 2.2.6.2, the position on the true orbit trails the position on the nominal orbit in the along-track direction. It follows that the true range will be longer than the range to the reference position. As a consequence, the orbit differences shown in Fig. 2.2.9 will result in $(O - C) > 0$ at satellite rise, but $(O - C) < 0$ when the satellite sets at the observing station's horizon. At some point during the pass over the station, the satellite motion will be perpendicular to the observer's viewing direction, so none of the along-track differences will be "seen"; that is, "O" goes to zero. If the pass has a lower elevation, the basic characteristics are the same, as shown for the low-elevation Fortaleza pass in Fig. 3.2.5.

3.3 CONCEPTUAL MEASUREMENT SYSTEMS

3.3.1 RANGE

All measurements of range are based on the *time-of-flight* principle. Simply stated, an instrument transmits a signal, usually with some appropriate time duration, which is reflected by a passive target or retransmitted by an active target. A *two-way range* may originate with an instrument located on the surface of the Earth, or *ground-based* instrument, and the signal will travel to the satellite and back to the transmitting site. One example of a two-way instrument is the satellite laser ranging (SLR) hardware, which is described in Section 3.5.2. In the SLR measurement, a laser pulse travels on an *uplink path* to the satellite, where it is reflected. The *downlink path* takes the signal from the satellite back to the transmitting site. The uplink and downlink paths constitute the two-way measurement. Some two-way range measurements may be transmitted and received at the same location by essentially the same instrumentation, but others may use a transmitter at one location and a receiver at another. This latter case is sometimes referred to as a *three-way measurement*, in spite of only uplink and downlink paths in the measurement. In some communities, the term *bi-static measurement* may be used.

The *one-way range* is based on the transmittal of a signal by a satellite or a ground-based transmitter that is received by separate instrumentation. If the transmit source is within the satellite, the signal may travel only a downlink path.

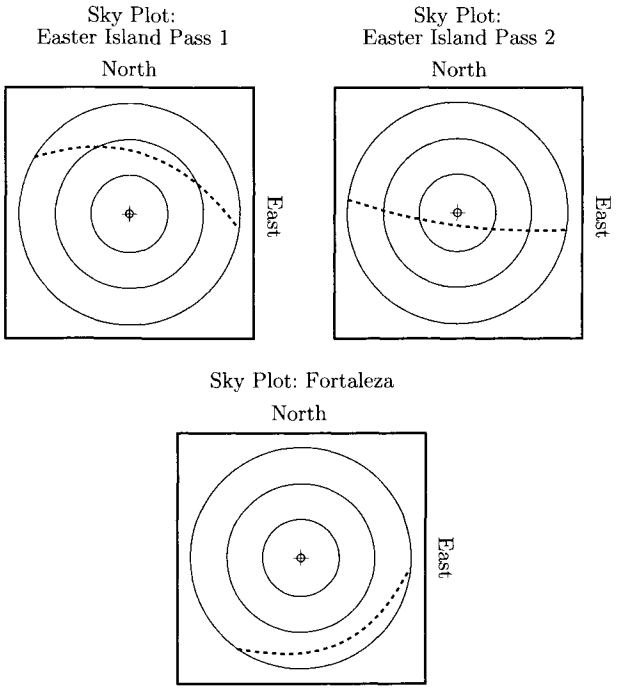

Figure 3.2.4: Sky plots. These plots illustrate the azimuth and elevation for the three passes shown in the ground track of Fig. 3.2.1. The circles represent increments of 30° elevation, with the outermost circle at 0° elevation and the center of the circles at 90° elevation. Azimuth is measured clockwise from north.

Alternatively, the transmitter could be ground-based, and the signal might be received by satellite-borne instrumentation on the uplink path. An important example of the satellite-borne transmitter is the Global Positioning System (GPS), discussed in Section 3.5.1. Even in the case of GPS, the receiver could be located on a satellite, rather than being ground-based.

One-Way Range

Assume a signal of very short duration is transmitted with a specific electromagnetic frequency at time t_T. The transmitted signal propagates along a path and arrives at a point instrumented to receive the transmitted signal. The signal arrives at the receiver at time t_R. Since the signal travels at the speed of light, denoted by c, the signal has traveled a one-way distance given by

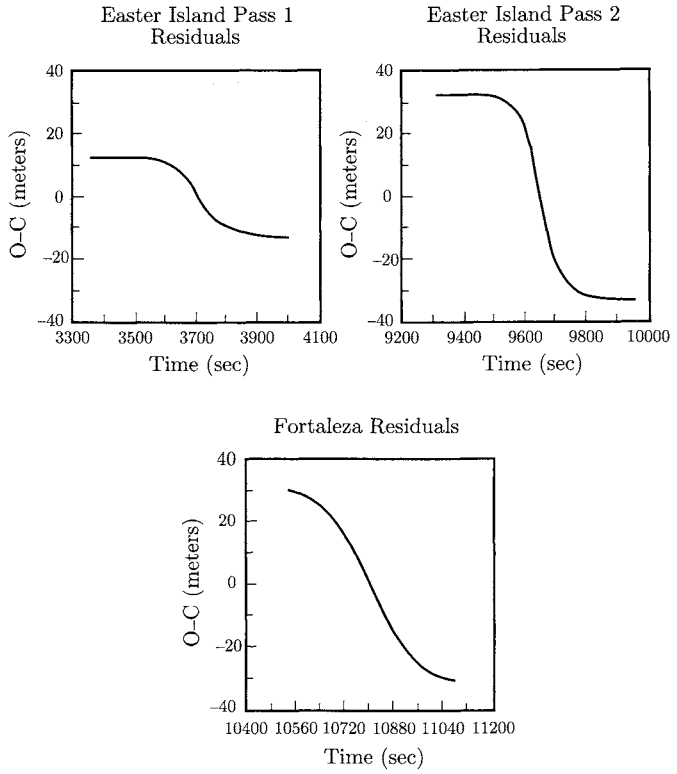

Figure 3.2.5: Range residuals vs time. The range residuals, $(O - C)$, for the three passes illustrate the effect of the orbit error shown in Fig. 2.2.9 on range residuals. The orbit used to generate O is Example 2.2.6.1 and the orbit used to generate C is Example 2.2.4.1.

$$\tilde{\rho} = c(t_R - t_T)\,. \tag{3.3.1}$$

Different clocks are used to register the respective times, t_R and t_T. If the clocks used to record t_R and t_T are precisely synchronized, then $\tilde{\rho}$ represents the true range, aside from other effects such as atmospheric delays of the signal propagation. For the discussion in this section, c will represent the speed of light in a vacuum. Unfortunately, the clocks used are generally not well-synchronized. In fact, if the clock used to determine the transmit time is running significantly faster than the receiver clock, the quantity $\tilde{\rho}$ could be negative! With the synchronization aspect in mind, the quantity $\tilde{\rho}$ generally will not represent the true range, but

it is related to the true range. As a consequence, $\tilde{\rho}$ is designated the *pseudorange*.

Using the GPS case as an example, a signal with special characteristics is transmitted. The time when this signal is transmitted is predetermined, but the actual time when the signal is emitted will be controlled by the satellite clock. The time of signal arrival at a reception site is measured by an independent clock. Let t represent *clock time*—time as registered by a clock—but let T represent true time. Everyday experience suggests that a reasonable model for the relation between clock time and true time is the linear relation

$$t = T + a + b(T - T_0) + \epsilon' \tag{3.3.2}$$

where a represents a constant offset of clock time from true time, b represents a linear clock drift, T_0 is a reference time, and ϵ' represents other errors, such as nonlinear terms and stochastic components. In essence, the linear clock model is assumed to be valid over the interval from T_0 to T. Applying Eq. (3.3.2) to both the transmitter clock and the receiver clock, the pseudorange becomes

$$\tilde{\rho} = c(T_R - T_T) + c(a_R - a_T) + c(b_R - b_T)(T - T_0) + \epsilon \tag{3.3.3}$$

where the subscript T refers to the transmitter clock, R denotes the receiver clock, and ϵ is the difference between the other error sources. Since the term $c(T_R - T_T)$ is the true range, it is evident that

$$\tilde{\rho} = \rho(T_T, T_R) + c(a_R - a_T) + c(b_R - b_T)(T - T_0) + \epsilon \tag{3.3.4}$$

where $\rho(T_T, T_R)$ is the distance between the transmit point at time T_T and the receive point at T_R; that is, the true range. Recall that the true range is distinctly different from the ideal range, which does not account for the finite speed of light. It is further evident that pseudorange differs from true range by the clock-related terms. Furthermore, if the time interval $(T - T_0)$ and the difference in drift terms are sufficiently small, then

$$\tilde{\rho} = \rho + c(a_R - a_T) + \epsilon \tag{3.3.5}$$

which illustrates that pseudorange is a *biased range*; the pseudorange differs from true range by a "constant" term (plus noise). Letting ρ_b represent $c(a_R - a_T)$, a range bias, it follows that

$$\tilde{\rho} = \rho + \rho_b + \epsilon\,. \tag{3.3.6}$$

This discussion has ignored the influence of other delays that contribute to the signal arrival time. In particular, atmospheric refraction will delay the signal (see Section 3.4.2) and contribute an additional term, $\delta\rho_{\text{atm}}$, to Eq. 3.3.5 to yield

$$\tilde{\rho} = \rho + \rho_b + \delta\rho_{\text{atm}} + \epsilon\,. \tag{3.3.7}$$

The one-way range instrumentation measures $\tilde{\rho}$ by determining t_T and t_R. Equation (3.3.7) shows that the measured quantity is a biased range. A useful alternate form of Eq. (3.3.7) is

$$\tilde{\rho} = \rho + c\delta t_R - c\delta t_T + \delta\rho_{\text{atm}} + \epsilon \tag{3.3.8}$$

where δt_R is the receiver clock correction and δt_T is the transmitter clock correction. For example, from Eq. (3.3.4), $\delta t_R = a_R + b_R(T - T_0)$ plus higher order and random components.

From Eq. (3.3.7) the measured quantity, $\tilde{\rho}$, is related to the satellite position at time T_T and the receiver position at time T_R, or

$$\tilde{\rho} = [(X - X_I)^2 + (Y - Y_I)^2 + (Z - Z_I)^2]^{1/2} + \rho_b + \delta\rho_{\text{atm}} + \epsilon \tag{3.3.9}$$

where (X, Y, Z) represents the true position of the satellite at time T_T and the true instrument components $(X, Y, Z)_I$ are determined at T_R.

A computed pseudorange, $\tilde{\rho}_c$, would be formed with an assumed, or nominal, ephemeris for the satellite and coordinates of the instrument and other parameters in Eq. (3.3.9). A *residual* would be obtained from the difference, $\tilde{\rho} - \tilde{\rho}_c$. Such a residual is required in orbit determination.

It is significant to note that the true range, ρ, is formed as the magnitude of the difference between two position vectors, each of which has a different time attached to it. As a consequence, these two vectors must be expressed in the same reference frame. If the reference frame is nonrotating, the resulting path is simply the straight line distance between the two vectors. If an Earth-fixed frame is used, for example, the path appears to be curved and it will be necessary to account for this curvature. Unless otherwise stated, it will be assumed that $\rho(T_T, T_R)$ will be formed using a nonrotating reference frame.

Table 3.3.1 shows the quantity $(\delta T = T_R - T_T)$ for transmitting satellites at different altitudes, assuming the satellite is at the zenith of a ground-based receiver. With $c = 299,792.458$ km/sec, the GPS case is $20,000 \div c = 0.08673$ sec.

Two-Way Range

The two-way range includes both an uplink and a downlink path, where the order will be dependent on the transmitter source. For this discussion, assume the transmitter to be located on the Earth's surface and the same instrumentation will be used to receive the return signal. For simplicity, assume no time delay exists when the signal arrives at the satellite and is retransmitted. This description matches the ground-based satellite laser ranging (SLR) instrumentation, where the transmitted laser pulse is reflected by the satellite back to the transmitting station. Another important example is a satellite altimeter, where the satellite-borne

Table 3.3.1:

One-Way $\delta T = T_R - T_T$ at Ground Observer Zenith

Transmitter	Altitude (km)	δT (millisec)
Shuttle	400	1.33
ERS-1	700	2.33
TOPEX/Poseidon	1336	4.46
GPS	20,000	86.73
Geosynchronous	36,000	140.10

altimeter emits a pulse in the satellite nadir direction and the pulse is reflected by the Earth's surface (e.g., the ocean) back to the satellite. For simplicity, assume the transmitted pulse has a Gaussian shape. A commonly used point on the pulse for determination of t_T is the centroid, but other points may be used that are determined by the hardware characteristics. The return pulse is usually characterized by lower energy, but if the return pulse is also Gaussian, the receive time, t_R, can be determined for the centroid. In the SLR case, the instrumentation records the time when the laser pulse was transmitted by the ground-based hardware, t_T, and the time, t_R, represents the time when some portion of that pulse returns to the transmitting site after being reflected by the satellite. Hence, the round-trip distance traversed by the pulse is

$$\rho_{rt} = c(t_R - t_T) \tag{3.3.10}$$

where the transmit and receive times are measured by the same clock, denoted by clock time, t. Since the path length is the round-trip distance, the two-way ranges corresponding to the examples in Table 3.3.1 will be double those shown.

As in the one-way example, assume the instrumentation clock can be characterized by a linear clock model, Eq. (3.3.2). It follows that

$$\rho_{rt} = c(T_R - T_T) + b(T_R - T_T) + \epsilon \tag{3.3.11}$$

where the offset term, a, has cancelled since it is assumed to be based on the same clock. If the clock drift is sufficiently small over the round-trip time interval and other clock error terms plus atmospheric delays can be ignored, then the round-trip range is essentially the true round trip distance. The removal of the major clock term, a, in the two-way range is a significant advantage for this measurement type.

As in the one-way range case, atmospheric delays must be considered. Assuming the drift term can be ignored, it follows that a more accurate representation of Eq. (3.3.11) is

$$\rho_{rt} = c(T_R - T_T) + \delta\rho_{\text{atm}} + \epsilon \tag{3.3.12}$$

where $\delta\rho_{\text{atm}}$ is the atmospheric delay contribution.

The orbit determination process will compare the measured range, ρ_{rt}, to a computed value based on t_T and t_R, a nominal satellite ephemeris and nominal ground station coordinates, plus modeled atmospheric contributions and other effects. A computed value of ρ_{rt} with this information is not straightforward, since the computation requires the time when the signal arrives at the satellite, but this parameter is not directly measured.

An iterative process can be invoked for the computed two-way range to determine the unknown time of arrival of the signal at the satellite. Two sets of iterations are required. For this discussion, assume that errors in clock time, t, are insignificant. Further assume that an ECI nominal satellite ephemeris is available and that an appropriate procedure is available to evaluate the ephemeris for any arbitrary time. It is also assumed that nominal coordinates of a ground-based ranging station are given in ECF, but the transformation between ECF and ECI is known. The following description of the iteration assumes that the signal propagates in a straight line path in the ECI frame (e.g., a very narrow laser beam); hence the description of the procedure is based on ECI.

If the measured signal transmit time, t_T, is taken as the starting point, then the computed two-way range can be determined as follows:

1. Determine the instantaneous range, ρ, between the station and the satellite at t_T using Eq. (3.2.3). This step requires evaluation of the ephemeris at t_T and the station coordinates in ECI, so the ECF coordinates are transformed into ECI using the ECF-to-ECI transformation matrix, Eq. (2.4.11).

2. Compute the approximate signal arrival time at the satellite as $t_a = t_T + \rho/c$.

3. Evaluate the ephemeris at t_a and compute the corresponding range, ρ_{new}, between the ECI satellite position at t_a and the ECI position of the station at t_T.

4. Compare ρ and ρ_{new}; if the difference is less than some specified criteria, such as 1 micrometer, then the process has converged and no more iterations are required. Otherwise, rename ρ_{new} to be ρ and go to step 2.

After converging on the computed signal arrival time, t_a, and the corresponding uplink range, ρ, the next set of computations determine the downlink range and time of arrival at the station based on the models. A procedure similar to the

one given earlier can be followed. In this case, the arrival time at the satellite will be assumed to be known from the first iteration, and the arrival time at the station is unknown. This arrival time will most likely differ from the measured arrival time because of errors in the nominal orbit, errors in the station coordinates, and mismodeling of the media corrections.

It turns out, however, that the preceding iterative process can be remarkably simplified. From the measured round-trip range, ρ_{rt}, the average range can be determined as $\rho_{\text{avg}} = \rho_{rt}/2$ and the approximate pulse arrival time at the satellite is $\rho_{rt}/(2c) = \delta\tau$. It follows that the satellite pulse arrival time is $t_a = t_T + \delta\tau$. If the instantaneous range is computed at t_a (evaluate the ephemeris and the ECI station coordinates at this t_a), this range is approximately equal to ρ_{avg}, at least to the submillimeter level. As a consequence, the measured round-trip range can be modeled by the instantaneous range (one-way) determined at the time t_a.

In the case of a satellite-borne altimeter, the two-way measurement originates with an instrument in the satellite, but the signal propagation is earthward, usually in the nadir direction defined by either the local geodetic vertical or the radial direction to the geocenter. In the altimeter case, the signal is reflected by the Earth's surface (e.g., the ocean). The preceding discussion in this section for the ground-based instrument applies as well to the altimeter. Let h_{rt} represent the round-trip altitude, and

$$h_{rt} = c(t_R - t_T) \tag{3.3.13}$$

where t_R is the signal transmit time and t_T is the receive time. Note that the measurement consists of a downlink path (satellite to surface) and an uplink path for the echo (surface to satellite). Even in the ECI coordinate system, the motion of the Earth has a small contribution to h_{rt} during the round-trip interval.

As in the case of the previous two-way range, the computed altitude requires an iterative process to determine the surface time of arrival. In the general case that allows for an off-nadir pointed altimeter, the process is similar to the preceding discussion for the ground-based two-way ranging station. The average altitude is

$$h_{\text{avg}} = h_{rt}/2 \tag{3.3.14}$$

and the average time is

$$t_{\text{avg}} = t_T + h_{\text{avg}}/c\,. \tag{3.3.15}$$

As in the preceding case, h_{avg} is a good approximation (submillimeter) to the instantaneous altitude formed at t_{avg}. The time of signal arrival at the surface is closely represented by t_{avg}.

Example

Consider a satellite in an equatorial posigrade, circular orbit with an altitude of 600 km above a spherical Earth. Assume the satellite is 20° in true anomaly

past the zenith direction of a two-way ranging station, which places the satellite at 4.3° elevation with respect to the station. Assume a signal is transmitted by the station at $t = 0$. The uplink iteration to determine the computed range gives 2393433.99356 meters, with signal arrival at the satellite 0.007983636445 sec after transmission. The downlink iteration gives 2393426.58799 meters and a signal arrival at the ground station 0.015967248187 sec ($\delta\tau$) after transmission. The average range (sum of uplink and downlink, divided by two) is 2393430.290775 meters. Determination of the instantaneous range at $\delta\tau/2$ (0.007983624094 sec) gives 2393430.290689 meters.

3.3.2 RANGE-RATE

Most *range-rate* systems in current use are based on a single propagation path, either uplink or downlink. The following discussion treats the problem from two viewpoints: an instrument transmitting a short duration pulse at a known interval and a beacon that transmits a signal with a known frequency.

Repeated Pulse Transmission

Assume a satellite-borne instrument transmits a pulse at a specified and fixed interval, δt_T. Hence, the pulses are transmitted at a sequence of times (e.g., t_{T1}, t_{T2}, etc). The transmitted pulses are received by a ground-based instrument and the arrival times are recorded as t_{R1}, t_{R2}, and so on, where t_{R1} is the arrival of the pulse transmitted at t_{T1}. The transmit and receive times are related by

$$\begin{aligned} t_{R1} &= t_{T1} + \rho_1/c \\ t_{R2} &= t_{T2} + \rho_2/c, \end{aligned} \tag{3.3.16}$$

and so on, where the relation to Eq. (3.3.1) is obvious. If t_{R1} is subtracted from t_{R2}, it follows that

$$t_{R2} - t_{R1} = \delta t_T + (\rho_2 - \rho_1)/c \tag{3.3.17}$$

or

$$\delta t = \delta t_T + \delta\rho/c \tag{3.3.18}$$

where $\delta t = t_{R2} - t_{R1}$ and $\delta\rho$ represents the *range change* between t_{T2} and t_{T1}. Consider the following cases:

- If $\rho_2 > \rho_1$: the length of the path traversed by the signal is getting longer (the transmitter and receiver are getting farther apart), then $\delta t > \delta t_T$. In other words, the time between successive pulse arrivals is longer than the fixed interval between their transmission, δt_T.

- If $\rho_2 < \rho_1$: the length of the signal path is getting shorter (the transmitter and receiver are moving toward each other), then $\delta t < \delta t_T$. In this case, the time between successive pulse arrivals is shorter than δt_T.

- If $\rho_2 = \rho_1$: there is no change in the signal path length and the pulse arrival interval equals the pulse transmit interval.

Equation (3.3.18) can be rewritten as

$$\delta t = \delta t_T(1 + (\delta\rho/\delta t_T)/c) \tag{3.3.19}$$

where $(\delta\rho)$ is the range change in the time interval δt_T. Hence, $\delta\rho/\delta t_T$ is a form of *range-rate*. If the ground-based instrument measures δt, it is evident that this measured quantity is dependent on the range change during the interval δt_T. Note that the measured quantity is not the instantaneous range-rate, although the shorter the interval δt_T, the closer the measured quantity will be to the instantaneous range-rate. In a sense, the previous description is a form of measurement differences, which is discussed later in this chapter. Since the same clock is used to determine the pulse transmit times and a separate clock is used to measure the pulse receive times, the quantities δt and δt_T are time differences based on the time recorded by separate clocks. As in the case of two-way ranging, the dominant clock model term, a, will cancel in the differencing process while the drift and higher order clock effects will remain at some level.

Transmitter Beacon

Assume a satellite contains a radio beacon that transmits a signal with a known frequency, f_T. The transmitted signal arrives at a ground-based site with an apparent frequency f_R, but this arrival signal is usually mixed with a reference frequency standard at the site. The arriving signal is multiplied with the reference frequency, f_G, which yields a signal that contains frequencies of $(f_G + f_R)$ and $(f_G - f_R)$. The sum of frequencies is filtered and if f_G is essentially f_T, the resulting $(f_G - f_R)$ signal represents the apparent change in transmitted frequency. The receiver is designed to count the number of cycles at this frequency between two times, t_{R_1} and t_{R_2}, thus

$$N_{1,2} = \int_{t_{R_1}}^{t_{R_2}} (f_G - f_R)dt \tag{3.3.20}$$

where $N_{1,2}$ represents the number of integer cycles plus the fractional part of a cycle in the measured frequency $(f_G - f_R)$ during the time interval between t_{R_1} and t_{R_2}. Let

$$t_{R_1} = t_{T_1} + \Delta t_1$$

and

$$t_{R_2} = t_{T_2} + \Delta t_2$$

where $\Delta t_1 = \rho_1/c$ and ρ_1 is the distance from the transmit point to the receive point at t_{R_1}. Assuming that f_G is constant,

$$N_{1,2} = f_G\left[t_{T_2} - t_{T_1} + (\rho_2 - \rho_1)/c\right] - \int_{t_{R_1}}^{t_{R_2}} f_R dt\,. \tag{3.3.21}$$

However, the last integral is

$$\int_{t_{R_1}}^{t_{R_2}} f_R dt = \int_{t_{T_1}}^{t_{T_2}} f_T dt = f_T\left[t_{T_2} - t_{T_1}\right]\,. \tag{3.3.22}$$

Thus,

$$N_{1,2} = (f_G - f_T)(t_{T_2} - t_{T_1}) + f_G(\rho_2 - \rho_1)/c\,. \tag{3.3.23}$$

Let $\delta t = t_{T_2} - t_{T_1}, \delta\rho = \rho_2 - \rho_1$, and f_G equal f_T, then

$$N_{1,2}/\delta t = (f_T/c)(\delta\rho/\delta t)\,. \tag{3.3.24}$$

It follows that

$$f_R = f_T - N_{1,2}/\delta t, \tag{3.3.25}$$

so the apparent received frequency is $f_T(1 - (\delta\rho/\delta t)/c)$, and it is evident that this frequency depends on the range-rate. In other words, Eq. (3.3.25) illustrates the *Doppler effect*. If the relative motion between the transmitter and receiver is positive (the two are moving apart), then $f_T - f_R$ is less than f_T; that is, the apparent frequency of the transmitter beacon is lower than the actual frequency. But if the relative motion is negative, the apparent frequency of the transmitter beacon is higher than f_T. These results are consistent with those in the preceding section for the repeated pulse transmission, as they should be since both cases are based on the Doppler effect. An important element of the preceding discussion is the fact that instantaneous range-rate cannot be measured. Instead, the measured quantity $(N_{1,2})$ is related to the range change $(\delta\rho)$ in a specified interval of time (δt). Depending on the realization of the previously described concept, the instrument design may measure $N_{1,2}$ by allowing the zero crossings of $(f_G - f_T)$ to increment a counter, thereby generating an integer count, or Doppler count. In some designs, the counter may reset at the end of the count interval (t_{R_2} in the previous discussion), or it may simply record the content of the counter at the interval end. In the continuous count case, the count is made with respect to some interval when the signal from the transmitter first appeared, where the start count may be nonzero.

Another interpretation of $N_{1,2}$ can be obtained by rearranging the terms in Eq. (3.3.23) to give

$$\rho_2 = \rho_1 + N_{1,2}\ c/f_G - c/f_G(f_G - f_T)(t_{T_2} - t_{T_1}), \tag{3.3.26}$$

which suggests that a range measurement can be formed from the measured $N_{1,2}$. In this representation, ρ_1 is not known so ρ_2 can be regarded to be a biased range, similar to the previously described pseudorange. If t_2 is any time after t_1, Eq. (3.3.26) demonstrates that $N_{1,2}$ exhibits a range-like variation with time. For these applications, $N_{1,2}$ is usually the accumulated integer cycles plus the fractional part of the cycle. Although the fractional part is the *phase*, the term is commonly used to describe the sum of the integer cycles plus the fractional part. In the case when $f_G = f_T$, it follows that Eq. (3.3.26) can be written as

$$\rho_2 = \rho_1 + \tilde{\rho}_{PH} \tag{3.3.27}$$

where $\tilde{\rho}_{PH} = \lambda N_{1,2}$, $\lambda = c/f_T$, the signal wavelength. The quantity $\tilde{\rho}_{PH}$ is a pseudorange formed from the phase, *phase pseudorange*.

3.4 REALIZATION OF MEASUREMENTS

3.4.1 CONSIDERATIONS

The preceding section provided a conceptual discussion of the commonly used observations with little consideration given to the actual instrumentation applied to the realization of those observations. Although the discussion referred to the transmission of signals, the characteristics of those signals and the effects of the atmosphere were not treated. All signals are transmitted using a region of the electromagnetic spectrum, spanning from radio frequencies to visible regions of the spectrum. The commonly used regions of the spectrum are identified using terminology established during the 1940s global conflict and are shown in Table 3.4.1. Depending on their frequency, the signals will be influenced differently by the atmosphere, as discussed in the next section. Current technologies used in orbit determination are summarized in the following sections.

3.4.2 ATMOSPHERIC EFFECTS

Measurements used for orbit determination that propagate through the Earth's atmosphere will experience refractive effects. These effects delay the signals and, for example, lengthen the apparent range. Account must be taken of these delays in most cases, though the overall effect is unimportant in cases with coarse accuracy requirements (e.g., km-level). Since the atmosphere consists of distinctive layers, the propagation effects can be discussed within the context of the two most influential layers: troposphere and ionosphere.

Table 3.4.1:

Electromagnetic Spectrum Regions for Satellite Transmissions

Band Category	Approx. Frequency Range (MHz)	Wavelength Range (approx. cm)
L–Band	1000–2000	30–15
S–Band	2000–4000	15–7.5
C–Band	4000–8000	7.5–3.75
X–Band	8000–12500	3.75–2.4
K–Band	12500–40000	2.4–0.75
Infrared	3×10^8	0.00010
Green	5.6×10^8	0.0000532

(Skolnik, 1990)

Troposphere

The troposphere, which extends from the surface to about 10 km, is the region of the atmosphere where most meteorological effects that influence the surface take place. A transition region known as the tropopause lies between the troposphere and the next layer, the stratosphere. The dominant refractive contributions from these regions are associated with the troposphere, so the effect is referred to as the *tropospheric delay*, even though the stratosphere accounts for about 20% of the total. For radio frequencies, the troposphere and stratosphere are electrically neutral, or a *nondispersive medium*. The propagation delay, $\delta\rho$, is

$$\delta\rho = 10^{-6} \int N ds \tag{3.4.1}$$

where ds is a differential length along the path, N is the *refractivity*

$$N = (n-1)10^6 \tag{3.4.2}$$

and n is the *index of refraction*. The refractivity is usually written as the sum of the two components

$$N = N_{\mathrm{d}} + N_{\mathrm{w}} \tag{3.4.3}$$

where the subscripts denote *dry* (d) and *wet* (w) components. The *dry component*, or *hydrostatic component*, accounts for about 90% of the total effect. It assumes

the atmosphere behaves consistently with the ideal gas law and that it is in hydrostatic equilibrium so that only the surface pressure needs to be known. Modeling of the *wet component* is more difficult because of variability in the partial water vapor pressure, so this correction is estimated from the tracking data or may be obtained from other instrumentation, such as *water vapor radiometers*. A commonly applied expression for frequencies less than about 30 GHz was given by Smith and Weintraub (1953)

$$\begin{aligned} N_{\mathrm{d}} &= 77.6(P/T) \\ N_{\mathrm{w}} &= 3.73 \times 10^5(\tilde{e}/T^2) \end{aligned} \tag{3.4.4}$$

where P is pressure in millibars (mb), T is temperature in degrees Kelvin, and partial water vapor pressure, $\tilde{e}$, is in mb, all measured at the surface. Evaluation of Eq. (3.4.1) has been treated by Saastamoinen (1972).

In the zenith direction, the tropospheric delay is about 2 meters at sea level, but the effect is dependent on the elevation angle of the viewing direction through the atmosphere. For example, at 10° elevation, the delay is about 12 meters. Mapping functions are usually adopted to map the zenith effect to any elevation angle. These mapping functions are fundamentally dependent on the cosecant of the elevation angle, but the complexity of the mapping functions varies.

Various methods are used to generate the propagation delay, including ray-tracing. The signal delay is predominantly dependent on the cosecant of the satellite elevation seen at the station. A frequently used expression for the tropospheric delay, $\Delta\rho_t$, is

$$\Delta\rho_t(El) = \tau_d m_d(El) + \tau_w m_w(El) \tag{3.4.5}$$

where τ represents the zenith delay, $m(El)$ represents a mapping function with elevation dependency and the subscript d is the dry component and w is the wet component. The simplest mapping function is

$$m(El) = 1/(\sin(El))\,. \tag{3.4.6}$$

For optical wavelengths, such as those used with lasers, the troposphere behaves dispersively. As a consequence, the delay is dependent on the wavelength of the signal. For laser ranging systems, a commonly used correction for troposphere delay is given by Marini and Murray (1973):

$$\Delta\rho_t = \frac{f(\lambda)}{f(\phi,H)}\,\frac{A+B}{\sin(El)+\frac{B/(A+B)}{\sin(El)+0.01}} \tag{3.4.7}$$

where

$$A = 0.002357P_0 + 0.000141e_0$$

$$
\begin{aligned}
B &= (1.084 \times 10^{-8}) P_0 T_0 K + (4.734 \times 10^{-8}) \frac{P_0^2}{T_0} \frac{2}{(3 - 1/K)} \\
f(\phi, H) &= 1 - 0.0026 \cos 2\phi - 0.00031 H \\
K &= 1.163 - 0.00968 \cos(2\phi) - 0.00104 T_0 + 0.00001435 P_0 \\
e_0 &= \frac{R_h}{100} \times 6.11 \times 10^a \\
a &= \frac{7.5(T_0 - 273.15)}{237.3 + (T_0 - 273.15)}.
\end{aligned}
\tag{3.4.8}
$$

El is the true elevation, P_0 is the atmospheric pressure at the laser site (mb), T_0 is the atmospheric temperature at the laser site (degrees Kelvin), e_0 is the water vapor pressure at the site (millibars), R_h is relative humidity (%), ϕ is the site geodetic latitude, and H is the height of the site above the ellipsoid (km). Note that $f(\lambda)$ is

$$
f(\lambda) = 0.9650 + \frac{0.0164}{\lambda^2} + \frac{0.000228}{\lambda^4} \tag{3.4.9}
$$

where λ is the laser wavelength in microns. For example, a ruby laser has a wavelength of 0.6943 microns and $f(\lambda)$ is 1.0000, whereas a green laser ($\lambda = 0.532$ microns) has $f(\lambda) = 1.02579$. At optical wavelengths, the wet component is small and usually ignored.

Other mapping functions have been developed for radio frequency measurements. For example, the MIT Thermospheric mapping function, known as MTT, has close functional similarity to the Marini-Murray function (Herring *et al.*, 1992):

$$
m(El) = \frac{1 + \frac{a}{1 + \frac{b}{1+c}}}{\sin(El) + \frac{a}{\sin(El) + \frac{b}{\sin(El) + \frac{b}{\sin(El)+c}}}} \tag{3.4.10}
$$

where the coefficients for the dry part, m_d, are

$$
\begin{aligned}
a &= [1.2320 + 0.0130 \cos\phi - 0.0209 H_s \\
&\quad + 0.00215(T_s - T_0)] \times 10^{-3} \\
b &= [3.1612 - 0.1600 \cos\phi - 0.0331 H_s \\
&\quad + 0.00206(T_s - T_0)] \times 10^{-3} \\
c &= [71.244 - 4.293 \cos\phi - 0.149 H_s \\
&\quad - 0.0021(T_s - T_0)] \times 10^{-3}
\end{aligned}
\tag{3.4.11}
$$

where T_s is surface temperature in °C, $T_0 = 10$°C, ϕ is the site geodetic latitude, and H_s is the height of the site above the reference ellipsoid. The coefficients for the wet part, m_w, are

$$\begin{aligned} a &= [0.583 - 0.011\cos\phi - 0.052H_s \\ &\quad +0.0014(T_s - T_0)] \times 10^{-3} \\ b &= [1.402 + 0.102\cos\phi - 0.101H_s \\ &\quad +0.0020(T_s - T_0)] \times 10^{-3} \\ c &= [45.85 - 1.91\cos\phi - 1.29H_s \\ &\quad +0.015(T_s - T_0)] \times 10^{-3} \end{aligned} \tag{3.4.12}$$

In very high-accuracy cases, azimuthal dependencies should be accounted for in the mapping function or measured with water vapor radiometers.

Ionosphere

The ionosphere is the portion of the atmosphere that is characterized by the presence of ions and free electrons. The ionosphere is most distinctive at altitudes above 80 km and consists of several layers, but not all of the layers are completely distinct. The ionosphere has no significant effect on signals with optical wavelengths (e.g., lasers). For radio frequencies, the ionosphere is dispersive and the signal time delay is dependent on the frequency, as well as the electron content along the signal path. Thus, the time delay δt at a frequency f is, to order $1/f^3$,

$$\delta t = \frac{\alpha}{f^2} \tag{3.4.13}$$

where α is related to the *TEC (total electron content)* along the path. The term α is positive for group delays (e.g., pseudorange) and negative for carrier phase. Since the ionospheric delay is dependent on frequency, transmission of signals at different frequencies allows removal of the ionosphere, at least to an acceptable level for orbit determination applications. Given a ranging code transmitted at two different frequencies, f_1 and f_2, this equation can be used to eliminate the TEC and obtain an ionosphere-free range, ρ_c. Using the linear combination of range measurements made with f_1 and f_2, ρ_c can be shown to be

$$\rho_c = \gamma_1\rho_1 - \gamma_2\rho_2 \tag{3.4.14}$$

where ρ_1 is the range measurement from f_1 and ρ_2 is the measurement from f_2, and

$$\begin{aligned} \gamma_1 &= \frac{f_1^2}{f_1^2 - f_2^2} \\ \gamma_2 &= \frac{f_2^2}{f_1^2 - f_2^2}\,. \end{aligned} \tag{3.4.15}$$

Significant changes in total electron content take place both spatially and temporally. Predictive ionosphere models may be used to correct single-frequency ranging data, but the highest accuracy is achieved with dual-frequency measurements. For measurement systems that operate in the L-band of the frequency spectrum (e.g., GPS with $f_1 = 1575.42$ MHz and $f_2 = 1227.60$ MHz), the ionosphere delay can be meter-level to tens of meters, depending on the TEC. Although the linear combination increases the measurement noise compared to the single-frequency measurement, the removal of the systematic effects associated with ionospheric variability is essential for high-accuracy applications. Appropriate estimation techniques can aid in smoothing the increased measurement noise produced by the linear combination.

3.4.3 General Relativity

As noted in Chapter 2, an Earth orbiter experiences a small relativistic precession of the perigee. In this section, the relativistic effects associated with various measurements (e.g., range or time delay) are described. These effects include the constancy of the speed of light, time dilation, gravitational frequency shifts, and the Sagnac effect. Further details for GPS are given by Ashby (2002).

Depending on the altitude, a clock (oscillator) in a circular orbit may beat fractionally faster or slower than a clock with identical characteristics on the surface of the Earth. This effect applies to systems such as GPS, Transit, and DORIS. In the case of GPS, this relativistic effect is usually accounted for by slightly lowering the satellite oscillator frequency to 10.229999999543 MHz to achieve the effective frequency of 10.23 MHz when the satellite is in orbit. It is evident that this effect does not apply to passive satellites, such as Lageos, with no on-board oscillators.

If the clock's orbit is not perfectly circular, the clock will vary about the mean frequency with the same period as the orbit. For a GPS satellite with an orbital eccentricity of 0.01, for example, this could lead to a navigation error of up to 7 m. The correction to the time offset is easily calculated from knowledge of the GPS satellite position and velocity from

$$\Delta t_r = \frac{2\mathbf{r} \cdot \mathbf{v}}{c^2}. \tag{3.4.16}$$

In a system of several massive bodies, the gravitational fields of these bodies will influence the arrival time of a signal traveling at the speed of light from a source. For Earth orbiters, a nonrotating inertial reference system tied to the center of mass of the Earth usually is used, and the relativistic effect of the Earth's mass is the only contributor. If the signal is transmitted from a position at a distance r_1 from the geocenter and received at a position that is a distance r_2, and ρ is the distance between transmitter and receiver, then the relativistic correction to the

time delay caused by the Earth is:

$$\Delta t_{\text{delay}} = \frac{2GM}{c^3} \ln \left[\frac{r_1 + r_2 + \rho}{r_1 + r_2 - \rho} \right]. \tag{3.4.17}$$

For low-altitude Earth satellites, the contribution from other celestial bodies is negligible. In the case of GPS, this correction is a few cm, but the effect mostly cancels in differenced measurements (see Section 3.6).

An additional relativistic effect is known as the Sagnac effect. When working in the ECI frame, the Sagnac effect is not applicable; the iteration to calculate the light-time accounts for the motion of the receiver clock during the time of propagation. The Sagnac effect is generally a concern only for high-precision time transfer between ground-based clocks via a satellite. Ries *et al.* (1991) describe the relativistic effects for orbit determination.

3.5 MEASUREMENT SYSTEMS

3.5.1 ONE-WAY RANGE

GPS

The basic concept of a one-way range was described in Section 3.3.1. As noted in that description, the one-way range is based on the time required for a signal to travel from a transmitter to a receiver. The wide use of GPS makes it a suitable example of the one-way ranging technique. Further details of GPS are given by Hofmann-Wellenhof *et al.* (1997) and Leick (2003).

The GPS consists of a constellation of satellites, developed by the U.S. Department of Defense. Each satellite broadcasts signals to support one-way ranging at radio frequencies using the following basic elements: a radio transmitter, a computer, a frequency standard (provides both time and frequency reference for radio transmissions), a transmit antenna, and a power source. The characteristics of the constellation in January 2000 are summarized in Table 3.5.1. The GPS satellites are organized into six orbit planes ($i = 55°$) with four or five satellites in each plane. Each satellite has an orbital period of 11 hours 58 minutes.

All GPS satellites use the same frequencies in the L-band: 1575.42 MHz (known as L_1) and 1227.60 (known as L_2). These frequencies are termed the *carrier frequencies*, which are 154 f_0 and 120 f_0, where $f_0 = 10.23$ MHz, the GPS fundamental frequency. A third civil frequency (known as L_5 at 1176.45 MHz) is being planned for future GPS satellites starting with Block IIF. A thorough discussion of the GPS signals can be found in Parkinson *et al.* (1996).

Table 3.5.1

GPS Constellation Status: 1 January 2000 00:00:00.000 GPS-Time

Orb./Plane & Position	PRN	S/C type	Clock	a (km)	e	i (deg.)	Ω (deg.)	ω (deg.)	$\omega + M$ (deg.)	λ_{AN} (deg.)	
A-1	09	IIA	Cs	26559.3	0.0098	54.0	175.7	32.3	103.0	127.0	−53.0
A-2	25	IIA	Cs	26561.7	0.0078	53.6	173.5	232.9	356.0	71.9	−108.1
A-3	27	IIA	Cs	26559.9	0.0137	53.9	174.7	198.3	212.2	1.1	−178.9
A-4	19	II	Rb	26560.0	0.0053	53.1	172.4	203.6	238.8	12.0	−168.0
A-5	08	IIA	Rb	26539.7	0.0086	54.8	178.2	102.1	148.2	152.2	−28.0
B-1	22	IIA	Rb	26559.9	0.0129	53.5	233.7	30.5	278.4	92.6	−87.4
B-2	30	IIA	Cs	26562.8	0.0056	54.1	235.7	83.8	3.5	137.2	−42.8
B-3	02	II	Cs	26561.3	0.0194	53.6	232.9	236.7	140.7	24.3	−155.7
B-4	05	IIA	Cs	26562.0	0.0019	53.7	234.0	9.5	38.6	153.3	−26.7
C-1	06	IIA	Cs	26558.9	0.0068	54.5	297.2	222.1	306.4	170.8	−9.2
C-2	03	IIA	Cs	26561.2	0.0010	54.1	294.8	72.8	207.5	118.6	−61.4
C-3	31	IIA	Cs	26561.7	0.0092	54.6	295.4	45.7	175.0	102.7	−77.3
C-4	07	IIA	Cs	26559.5	0.0109	54.6	295.4	239.7	75.1	53.6	−126.4
D-1	24	IIA	Rb	26561.1	0.0090	56.5	358.4	261.4	325.4	61.7	−118.3
D-2	15	II	Cs	26555.5	0.0073	56.3	0.2	85.8	118.6	139.2	−40.7
D-3	17	II	Cs	26558.9	0.0113	56.4	2.5	167.5	224.5	14.7	−165.3
D-4	04	IIA	Rb	26562.0	0.0053	56.0	357.8	323.0	0.5	78.4	−101.6
D-5	11	IIR	Cs	26559.3	0.0029	53.0	355.2	189.8	101.0	125.8	−54.2
E-1	14	II	Cs	26562.4	0.0005	56.1	59.3	129.5	31.4	155.0	−25.0
E-2	21	II	Cs	26559.9	0.0160	55.7	56.9	211.5	130.0	22.5	−157.5
E-3	10	IIA	Cs	26557.3	0.0038	55.8	56.5	353.0	256.6	84.7	−95.3
E-4	23	IIA	Cs	26562.3	0.0145	55.9	59.2	249.3	163.6	41.8	−138.2
E-5	16	II	Cs	26562.3	0.0044	55.9	59.5	19.6	355.5	137.2	−42.8
F-1	01	IIA	Cs	26568.4	0.0048	55.0	117.9	258.8	335.0	5.7	−174.4
F-2	26	IIA	Rb	26562.3	0.0116	55.2	116.9	2.1	180.0	106.9	−73.1
F-3	18	II	Cs	26559.2	0.0076	54.4	114.0	107.0	117.9	162.7	−17.4
F-4	29	IIA	Rb	26558.6	0.0073	55.0	115.3	248.2	81.0	56.3	−123.7
F-5	13	IIR	Rb	26558.7	0.0022	55.2	116.5	322.6	244.1	138.7	−41.3

The osculating orbit elements are expressed in J2000, PRN is the GPS identifier, Cs denotes cesium and Rb is rubidium, S/C Type identifies the satellite design type, and λ_{AN} is longitude of the ascending node.

The discussion in this section also applies to the current Russian navigation satellite system, known as GLONASS (Global Navigation Satellite System) and the future European Space Agency GALILEO (planned for operation by 2008).

Both satellite constellations use three orbital planes with about 10 satellites (including spares) in each plane (GALILEO). The GLONASS satellites use a 63° inclination and orbit periods of 11 hours 15 minutes. GALILEO satellites are expected to use a 56° inclination with an orbit period of 14 hours 22 minutes. Each GLONASS satellite broadcasts on a different frequency in the L-band, but GALILEO will have broadcast characteristics similar to GPS.

A Block II GPS satellite is illustrated in Fig. 3.5.1. The transmit antenna is the array shown on the main body of the spacecraft with the helical windings. The large panels on both sides are the solar panels used to generate power. Each satellite carries standard quartz frequency standards, as well as multiple atomic frequency standards (two cesium and two rubidium). In fact, a tunable quartz standard is used to excite the cesium standard, for example, at the natural frequency of $9,192,631,770$ Hz. It is this frequency that, in fact, defines the SI second.

The carrier frequencies are derived from the frequency standard in use (cesium, rubidium, or quartz), but additional information is superimposed. A simple analogy can be drawn with a common radio where a carrier frequency is used (e.g., 100 MHz) to carry the audio ($< 20,000$ Hz). In this example, the transmitter superimposes audio on the carrier, and the receiver extracts the audio signal when the radio is properly tuned to the carrier frequency. In the case of GPS (or GLONASS), the information superimposed on the carrier includes ranging codes and other data necessary to perform the navigation function offered by the satellite constellation.

GPS uses several ranging codes, though they have many similarities. In concept, the ranging codes are generated as *pseudo-random noise* (PRN). Consider the PRN code to be a series of binary digits (bits)—001101011100—for example, superimposed on the carrier. Each bit, known in GPS terminology as a *chip*, has a specific time duration depending on the code. The PRN bit sequence is determined by a documented algorithm. Each bit in the sequence will be transmitted by the satellite at a specific time determined by the satellite clock (which is derived from the frequency standard). Hence, as the receiver extracts the bit sequence from the carrier, it will assign receive times to each bit based on its own clock. With the ability to replicate the PRN code, the receiver will cross-correlate, or align, the received bit sequence with the sequence it is able to generate. Since each bit has a known transmit time, the difference between receive time and transmit time is obtained by this cross-correlation; that is, the quantity $t_R - t_T$ in Eq. (3.3.1) is determined, as well as the individual times, t_R and t_T. Note that the time when each bit in the code is transmitted is determined by the satellite clock, so the time t_T is based on the satellite clock. Similarly, the time when the bit is

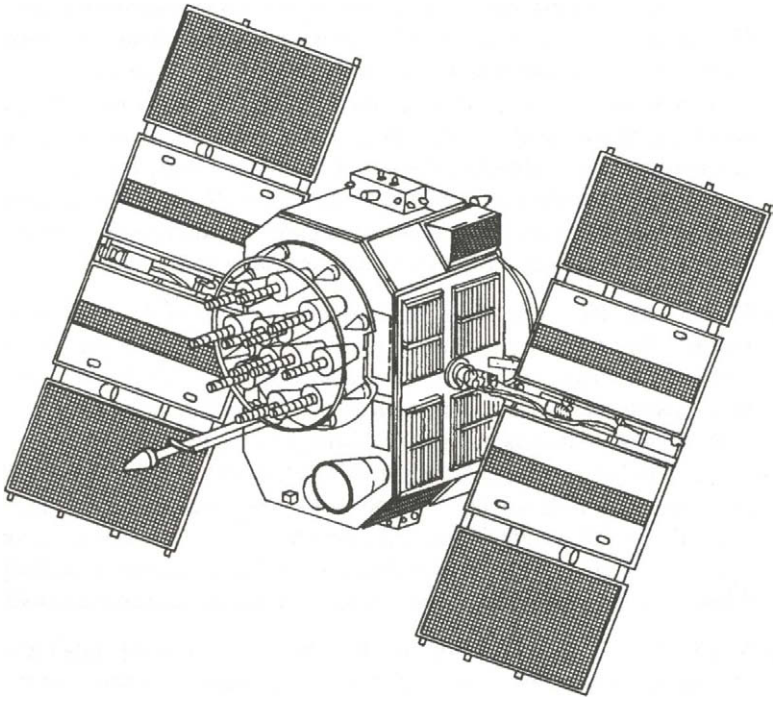

Figure 3.5.1: Block II GPS satellite. The satellite solar panels rotate about the axis mounted perpendicular to the main body (spacecraft bus) and the transmit antenna array, shown with the helical windings in the center, is directed toward the Earth's center. The antenna transmit pattern encompasses the visible Earth. A body-fixed set of axes includes a y axis coincident with the solar panel axes and a z axis directed toward the Earth's center. The spacecraft can present the maximum cross-sectional area of the solar panels to the Sun by rotating the bus about the z axis (yaw) and rotating the solar panels about the y axis.

received, t_R, is determined by the clock in the receiver.

The PRN codes currently transmitted by the GPS satellites are:

- C/A (Coarse Acquisition): This code uses 1023 bits and repeats every 1 ms. The algorithm for generating the sequence is described in detail by Hofmann-Wellenhof *et al.* (1997). Each bit requires about 1 microsec for transmission or about 300 meters in distance. One major purpose of this code is to facilitate acquisition of the P-code, which is a much longer bit sequence. Since the C/A code repeats every millisecond, an ambiguity exists between each millisecond interval. In other words, there is no information about absolute time within the C/A code. Resolving this ambiguity to determine the correct time interval requires additional information (e.g., information broadcast by the GPS satellites about their position).

- P (Precise): This code has a much longer duration of 37 weeks before it repeats. But this long repeat interval is divided into one week segments and each segment is assigned to a specific GPS satellite. Each satellite, in turn, repeats its assigned code each week. The duration for each bit is the equivalent of 30 meters in distance, corresponding to a transmission rate of 10.23×10^6 bits per sec. All information about the P-code is readily available. Most receivers use the C/A code for initial acquisition, then transition to the P-code. Since the P-code within each satellite does not repeat for one week, direct cross-correlation without use of the C/A code is challenging. Direct P-code acquisition is easier if the receiver has an accurate clock.

- Y: This code is generated from the P-code, but a classified code (W-code) is used to mix with the P-code. This mixing produces an encrypted P-code. When the Y-code is being transmitted, it is said that *Anti-Spoofing* (AS) has been invoked. The terminology arises from the military consideration that an adversary could transmit false P-code signals to confuse, or spoof, a receiver. When AS is used, the classified Y-code avoids this possibility.

In the GPS satellites known as Block II, including Block IIA and Block IIR, the C/A code is transmitted only on L_1 and the P/Y codes are transmitted on both L_1 and L_2. As a consequence, receivers capable of operating with only C/A are single-frequency receivers. Without the second frequency, the ionosphere correction cannot be made as accurately as measurements obtained with two frequencies, since it must rely on less accurate ionosphere models. Modern dual-frequency receivers are available that may be capable of correlating directly with the Y-code or they may use signal processing techniques, such as cross-correlation of the Y-code on the two frequencies to obtain the ionosphere delay. The method based on advanced signal processing effectively provides a dual-frequency measurement without knowledge of the Y-code. A pseudo-measurement usually is created by adding the measured ionosphere delay to the C/A pseudorange.

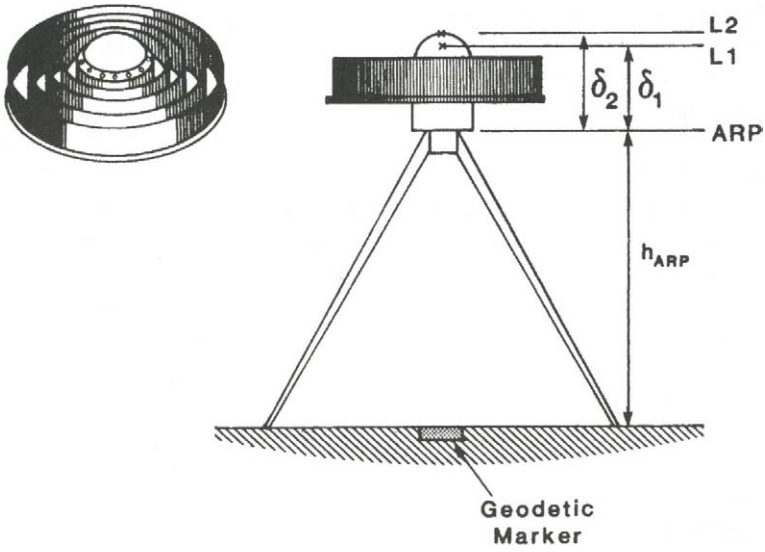

Figure 3.5.2: Typical GPS antenna setup. A choke-ring antenna is shown on the left and the antenna set up with a tripod over a geodetic marker is shown on the right. The height of the antenna reference point (ARP) above the geodetic marker is usually made to high accuracy with a geodetic-quality graduated ruler. The antenna phase center locations, denoted by L1 and L2, are separately calibrated.

A typical GPS receiver antenna installation is shown in Fig. 3.5.2, which shows a *choke-ring antenna* on the left. The choke ring is designed to reduce the effects of *multipath*, a phenomenon that occurs when the incoming GPS signal is reflected from nearby objects, such as buildings for a ground receiver. The reflected signal travels a longer path to the antenna, thereby introducing another error source into the measured signal. The choke-ring antenna is used for both ground-based and space-borne installations.

The relationship between the measured ranges and the satellite state requires the specification, or estimation, of the receiver antenna location. For precision orbit determination, the coordinates of the antenna shown in Fig. 3.5.2 must be known or determined in an appropriate reference frame. Furthermore, the reference point to which those coordinates refer and the specific point to which the range measurements are made are required. The antenna usually is described with a *phase center*, the point to which range measurements refer. This phase center usually is obtained by empirical testing, including testing in anechoic chambers. Such testing determines the phase center pattern for a particular antenna. Experi-

ence has shown that such patterns are common to a particular antenna type so that the test results of a subset may be applied to other nontested antennas.

For some antennas, the phase center pattern may be azimuthally symmetric, but may exhibit change as a function of elevation. For precision applications, the characteristics of the phase center variation must be known, as well as the location of the phase center even if it is invariant. Furthermore, in some cases, the coordinates published for a particular antenna may refer to a specific point other than the phase center, usually referred to as the *antenna reference point* (ARP). In these cases, the correction to the phase center must be separately applied. It is important that the specific point where *a priori* coordinates for the antenna should be applied is understood. To further complicate matters, the phase center for L_1 is usually different from the location for L_2. As shown in Fig. 3.5.2, the location for the L_1 phase center is δ_1 with respect to the ARP and the location of the L_2 phase center is δ_2.

The precision of GPS pseudorange measurements is receiver dependent, but most modern receivers are at the level of about 1 meter for P-code pseudorange. Note that the combination of two measurements made at different frequencies to remove ionosphere effects will produce a noisier measurement (Eq. 3.4.14). Although the precision of the pseudorange is meter level, the accuracy of the measurement is usually not comparable. For example, pseudorange measurements may be negative because of unsynchronized clocks, a clear indication that a measurement may be precise, but not accurate. Nevertheless, the correction for clock errors can be determined through appropriate estimation strategies and the corrections obtained from them will render the measurement accurate, as well as precise. As a means to control the accuracy of pseudorange measurements, the GPS satellite clocks may be *dithered*. This dithering produces clock errors that cannot be accounted for without access to Department of Defense classified information. When clock dithering is activated, it is said that *Selective Availability* (SA) has been invoked. Unclassified techniques to remove SA will be described in Section 3.6, but SA was deactivated in May, 2000.

The pseudorange measurement given by Eq. (3.3.9) can be expanded for either L_1 or L_2 to give

$$\tilde{\rho} = \rho + c(\delta t_R - \delta t_T) + \delta\rho_{\text{trop}} + \delta\rho_{\text{ion}} + \epsilon \tag{3.5.1}$$

where

$\tilde{\rho}$ is the measured pseudorange,

ρ is the true range between the true transmit time and the true receive time,

δt_R is the receiver clock difference with true time,

δt_T is the transmitter clock difference with true time,

$\delta\rho_{\text{trop}}$ is the troposphere delay,

$\delta\rho_{\text{ion}}$ is the ionosphere contribution, and

ϵ represents remaining errors, such as instrument noise.

Computation of the true range, ρ, would require knowledge of the true GPS satellite position and the true receiver antenna coordinates, as well as the true transmit and receive times. In practice, these quantities may not be known with high accuracy. In the orbit determination problem, for example, the satellite position may be known *a priori* with an accuracy of several meters. In this instance, the error term ϵ will represent the error between the true range and the computed range formed from the *a priori* known position. The receiver ability to measure pseudorange is characterized by the instrument's precision, usually at the meter level.

A more precise GPS measurement is based on the carrier phase. With the previously described atmospheric effects, the usual form of the phase, expressed as range and similar to Eq. (3.5.1), can be obtained from Eq. (3.3.26). For either L_1 or L_2, it can be shown that

$$\Phi = \rho + c(\delta t_R - \delta t_T) + \lambda\widetilde{N} + \delta\rho_{\text{trop}} - \delta\rho_{\text{ion}} + \epsilon \tag{3.5.2}$$

where

Φ is the measured phase range for the specified frequency,

λ is the wavelength of the signal (L_1 or L_2),

$\widetilde{N}$ is the integer phase ambiguity,

and the other terms were defined with Eq. (3.5.1).

Note that the raw phase measurement, ϕ, provided by a receiver consists of the accumulated integer cycles since a reference time, plus the fractional part of a cycle. The measured phase range is

$$\Phi = \lambda\phi \tag{3.5.3}$$

but in some receivers the expression may require $\Phi = -\lambda\phi$.

For comparison with pseudorange, the precision of phase range is usually characterized at the several millimeter level. If the GPS receiver is carried on a satellite, the term $\delta\rho_{\text{trop}}$ is zero and $\delta\rho_{\text{ion}}$ may be sufficiently small to neglect. Even at 1000 km altitude, the ionosphere contribution is at the decimeter level. The phase range from L_1 and L_2 can be combined to remove the ionosphere contribution using the same approach applied to pseudorange (Hofmann-Wellenhof *et al.*, 1997).

In applications of GPS measurements to the determination of an orbit of a low Earth orbiter (LEO), such as described in Section 3.7, the positions of the GPS satellites must be known or determined. One option is to apply the techniques of estimation described in the following chapters to the determination of the orbits of the GPS satellites using a network of ground stations. In some cases, the GPS satellite orbits may be determined simultaneously with the orbit of a LEO, but in others the GPS satellite orbits may be fixed to orbits determined by other sources.

The GPS ephemerides can be recreated using information broadcast by the satellites in near real time. These *broadcast ephemerides* can be generated from 16 parameters (*navigation message* or *ephemeris parameters*) based on Keplerian orbit elements and coefficients of terms that represent time dependency (see Hofmann-Wellenhof *et al.*, 1997) . The set of broadcast parameters applies to a specific interval of time, typically two hours, and new sets of parameters are broadcast automatically by a GPS satellite as the applicable time interval changes. The accuracy of the broadcast ephemerides generally is regarded to be at the 10-meter level. The primary intent is for the broadcast ephemerides to support real-time or near real-time applications. The information used to create the parameters broadcast by the GPS satellites is based on determination of the GPS satellite orbits by the Department of Defense using a set of six monitor stations. These monitor stations record pseudorange and carrier phase measurements between the ground-based receiver and the GPS satellite, which are then used to determine the orbits through a process that makes use of the methodologies in the following chapters. The orbits determined by this process are then extrapolated forward in time and the extrapolated ephemerides are approximated with a model based on the 16 ephemeris parameters. The ephemeris parameters are uploaded to the GPS satellites for broadcast during the appropriate time interval.

Precise GPS ephemerides are available with a latency of about one day or longer. These ephemerides are intended to support applications with high accuracy requirements, such as those related to space geodesy. Depending on the application, the position accuracy of a satellite carrying a GPS receiver may approach the centimeter level, while other applications may require an accuracy of ten meters. Two sources of ephemerides are available: *National Imagery and Mapping Agency* (NIMA) and the *International GPS Service* (IGS). In both cases, the respective agency operates a ground network of GPS receivers to support the determination of the GPS orbits. In the case of the IGS, an international collaboration of agencies supports a ground network of 200 receivers, somewhat uniformly distributed around the Earth. Seven Analysis Centers of the IGS use a subset of measurements from these receivers to determine GPS ephemerides and the IGS combines these products into a single official IGS product. The IGS final product is available with a latency of two to three weeks with an accuracy expected to be at the decimeter level, but a rapid product is available with a one-day latency.

Satellite-to-Satellite Tracking (SST)

Various forms of *satellite-to-satellite tracking* (SST) are in use. This terminology usually applies to measurements collected between a pair of satellites, but the common terminology enables identification of the respective satellite altitude. If a GPS receiver is carried on a LEO satellite, then the previously described GPS measurements would be categorized as *high-low* SST measurements. For some GPS satellites, an inter-satellite range measurement is made, known as *cross-link ranging*, that would be a *high-high* SST measurement.

A recent example of *low-low* SST measurements is represented by the *Gravity Recovery And Climate Experiment* (GRACE). The SST measurements are primarily used to detect components of the Earth's gravitational field and especially gravity variations associated with redistribution of mass. Two low-altitude satellites are used and each satellite transmits signals at two frequencies in the K-band (24 GHz) and Ka-band (32 GHz), but the actual frequencies used by each satellite are not identical. The satellites have approximately the same 500-km altitude and are in the same orbit plane, but separated in the along-track direction by about 200 km. Each satellite carries a GPS receiver, but these receivers have been modified to track both the GPS signals and the K-band signals transmitted by the other GRACE satellite.

The GRACE SST measurements in the K-band are similar to GPS one-way measurements of carrier phase made in the L-band. Two K-band measurements are made at different frequencies on each satellite to enable a correction for the ionosphere using the technique discussed in Section 3.4.2. The measurements made and recorded by each GRACE satellite are a form of one-way carrier phase similar to GPS. Each GRACE satellite carries an ultra-stable oscillator as the frequency reference ($\sim$4.8 MHz) that is used to generate the transmitted signal and to mix with the signal that arrives from the other satellite. Simply stated, each satellite measures the carrier phase signal it receives from the other satellite relative to the signal that it transmits. In an approach similar to measurement differencing (Section 3.6), the measurements collected on each satellite can be added to obtain a measurement that is proportional to the range between the satellites, while at the same time removing long-term oscillator instability. This form of SST measurement has been termed *dual-one-way-ranging*. The measurement and instrumentation has been described by Dunn *et al.* (2003).

3.5.2 Two-Way Range

SLR

The basic concept of a two-way range was described in Section 3.3.1. Examples of this measurement type include ground-based *satellite laser ranging* (SLR) systems and *satellite-borne altimeters*. SLR was applied for the first time by

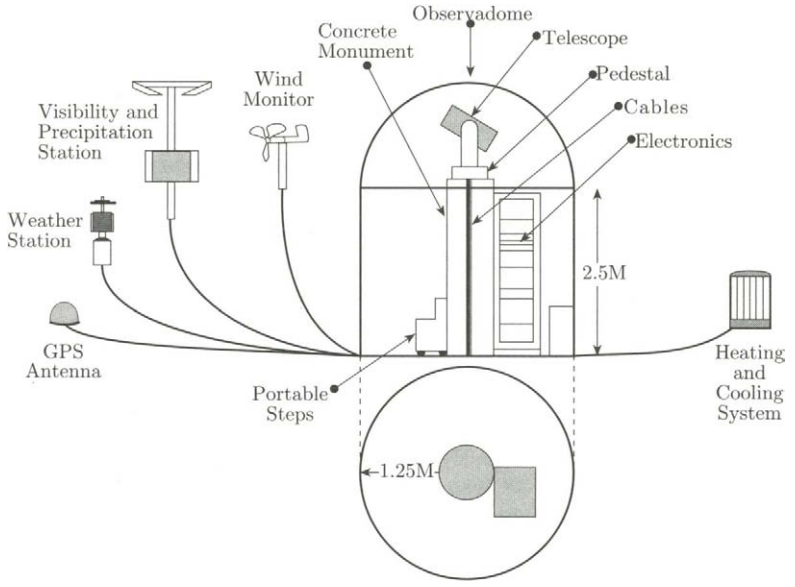

Figure 3.5.3: The illustrated SLR-2000 is designed for autonomous operation, whereas previous designs have required operators. The SLR concept is based on the measurement of time-of-flight between laser pulse transmission and receipt of echo photons. The telescope collects the echo photons and the electronics provide the time-of-flight (Degnan and McGarry, 1997).

NASA Goddard Space Flight Center in 1965 to Explorer 22 (Beacon Explorer-B).

Modern SLR stations use a Nd:YAG (neodymium yttrium aluminum garnet) laser to illuminate a satellite, usually at 0.532 micrometers (green). SLR systems rely on specially designed cube corners to reflect the incoming laser light back to the source, where a telescope collects the returning photons to measure the round-trip time from pulse transmission to pulse reception. Since lasers operate in the optical wavelengths, their operation will be dependent on local weather conditions. Nevertheless, the optical cube corners carried on a satellite to support SLR are simple and completely passive.

After conversion into a distance, the question arises for purposes of the computed range: what does the measured distance represent? Clearly, the range is measured to the cube corner on the satellite that reflected the arriving photons, but the originating point in the SLR may be more complex. In some cases, the distances of the laser paths within the instrument are carefully measured and a

correction to some adopted reference point is made. In other cases, the instrument may be used to range to a calibration target at a very precisely (and independently) measured distance to derive a correction to an adopted reference point. As a consequence, a range measurement represents the distance from some adopted reference point within the SLR system to a cube corner on the satellite.

The collimated laser beam has a divergence with a diameter of a few hundred meters at satellite altitude; hence, the satellite must be within the beam to achieve a successful echo. Errors that contribute to the satellite's position with respect to the laser beam include (a) satellite position prediction and (b) the instrument's telescope mount.

Position prediction errors result from the generation of a predicted ephemeris, usually obtained from the solution of the satellite equations of motion (e.g., Eq. 2.3.46) with a specified initial state. The initial state usually is determined from the application of the estimation techniques described in later chapters. The resulting ephemeris can be expected to contain errors from uncertainties in the force parameters in the equations of motion (e.g., the value of the drag coefficient), errors in the force modeling, and errors in the initial conditions.

In some systems, the position prediction errors are exceeded by errors in the telescope mount, which contributes to the laser pointing direction. In such cases, an adaptive search technique may be applied during the tracking pass to compensate for all of these errors.

A concept under development by NASA for an autonomous system is illustrated in Fig. 3.5.3, known as SLR-2000, which is expected to be deployed around 2005 (Degnan and McGarry, 1997). In the SLR system, the predicted ephemeris is used to drive the laser/telescope pointing. A clock is an essential element, although different clocks may be used. A time-interval counter or an event timer is used to measure time over the short duration between the emission of the transmit, t_T, pulse, and the reception of the echo pulse, t_R. A second clock, usually synchronized to GPS-Time using a time-transfer receiver, provides the absolute time required for time tagging the measurement.

The *International Laser Ranging Service* (ILRS) coordinates the global operation of independent SLR stations. The global network of SLR stations is supported by national agencies, and the recorded data from these stations are made available with a few hours latency through the ILRS data centers. The range data are regularly used to monitor geocenter motion and Earth orientation, and to determine SLR station velocities.

Several satellites have been designed to support SLR geodetic science. These satellites are spherical with a small area-to-mass ratio to reduce the effects of nongravitational forces. The relation of target cross-section to altitude is evident by the characteristics of the three satellite pairs summarized in Table 3.5.2. The solution of the satellite equations of motion (Eq. 2.3.46) provide the position of the satellite center of mass in an appropriate reference frame, but the SLR measure-

Table 3.5.2:

Geodetic Satellite "Twins"

Satellite	Launch	Diameter (cm)	Mass (kg)	a (km)	e	i (deg)
Starlette	1975 France	24	47	7326	0.020	50
Stella	1993 France	24	48	7184	0.001	99
Lageos-I	1976 U.S.	60	411	12254	0.005	110
Lageos-II	1992 U.S./Italy	60	405	12145	0.010	53
Etalon-I	1989 Soviet Union	129	1415	25514	0.001	65
Etalon-II	1989 Soviet Union	129	1415	25490	0.001	65

Lageos: LAser GEOdynamics Satellite

Etalon satellites are in GLONASS orbit planes

ments are made to the outer surface of the satellite, so a correction to the measured range for satellite center of mass is required. This correction is essentially the radius of the sphere, though in a precise sense it will account for the effective radius based on the laser pulse interaction with the cube corners.

Nonspherical satellites, such as TOPEX/Poseidon and ICESat, carry arrays of cube corners to support SLR tracking. These arrays usually mount the cube corners in some hemispheric-like pattern to enable ranging returns from the expected SLR directions. The array carried on ICESat is shown in Fig. 3.5.4. The necessary corrections from the SLR array optical center to the satellite center of mass are obviously more complicated than those for a spherical satellite.

The single shot precision of modern SLR systems is better than 1 cm, which is usually representative of the measurement accuracy from the hardware viewpoint. Another interpretation of accuracy, however, involves the application of all corrections in the orbit determination process. Orbits determined for Lageos-I from SLR, for example, usually are characterized with an accuracy at the centimeter level, in an RMS sense.

PRARE

Another modern two-way ranging system was developed in Germany and carried for the first time on the European Earth Resources Satellites (*ERS*), known as ERS-1 and ERS-2. *PRARE* (Precise Range and Range Rate Equipment) places the primary transmitter and receiver in the satellite, but ground stations have both transmit/receive functions as well. Two signals are transmitted by the satellite-borne PRARE, one at 2.2 GHz (S-band) and the other at 8.5 GHz (X-band), and

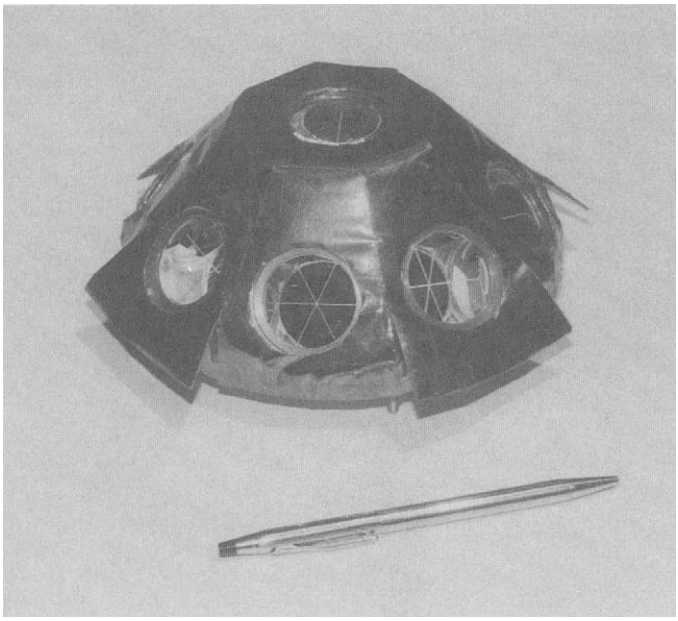

Figure 3.5.4: The ICESat SLR array. The circular components on each flat face contain a cube corner with the optical property of reflecting incoming light back to the source. There are nine corner cubes, each with a diameter of 3.2 cm. (Photo courtesy of ITE, Inc.)

both signals have a PRN code imposed. The time delay between the two frequencies is determined by the ground receiver and transmitted to the satellite. The received X-band signal is retransmitted to the satellite on a 7.2-GHz carrier frequency with the PRN code. A two-way range is obtained in X-band by measurement of the transmit and receive times of the X-band signal. The ionosphere correction is applied with the ground-transmitted determination based on the downlink signal. A one-way Doppler measurement is also made using the X-band.

Altimeter

A radar altimeter, such as those carried on TOPEX/Poseidon (T/P), operates similarly to the SLR system as a two-way measurement. The altimeter sends a chirp and measures the round-trip time. The TOPEX altimeter (U.S.) operates with two frequencies to enable a correction for the ionosphere, whereas the Poseidon altimeter (France) uses a single frequency and relies on other data to pro-

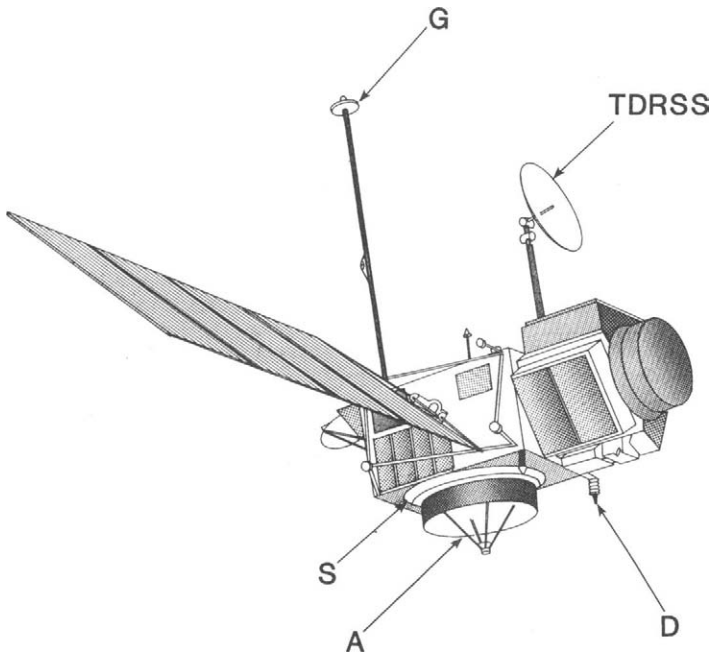

Figure 3.5.5: The TOPEX/Poseidon satellite. The radar altimeter antenna (A) is directed toward the Earth (nadir direction), the DORIS receiver antenna is D, the SLR array (S) consists of corner cubes mounted on the circumference of the altimeter antenna, the GPS receiver choke-ring antenna (G) is mounted at the end of a long boom to reduce multipath effects, and the TDRSS antenna is shown.

vide the ionosphere correction. The TOPEX frequencies are 13.6 GHz and 5.3 GHz, and the Poseidon frequency is 13.65 GHz. The altimeters share a common antenna, but only one altimeter is operated at a time. The TOPEX ionosphere correction can be obtained from Eq. (3.4.12), and the antenna is shown in Fig. 3.5.5. As shown, TOPEX carried several tracking systems that supported determination of the TOPEX orbit.

Laser altimeters, such as the *Mars Orbiter Laser Altimeter* (MOLA) and Earth-orbiting versions (such as the *Geoscience Laser Altimeter System*, or GLAS, carried on ICESat), function similarly to SLR. Both MOLA and GLAS operate with a near-infrared Nd:YAG wavelength of 1064 nanometers.

TDRSS

It is apparent from the discussion in Section 3.2.4 that tracking measurements collected by ground-based instrumentation will be limited to those time periods when the satellite is above the horizon at the ground location. For a low-altitude satellite, say 1000 km, such viewing opportunities will be limited to a few passes per day, with an individual pass duration of about 10 minutes or less. On the other hand, an appropriately positioned geosynchronous satellite always remains above a ground station's horizon and the geosynchronous satellite will have a very broad region to view the low-altitude satellite. The *NASA Tracking and Data Relay Satellite System* (TDRSS) takes advantage of this latter characteristic by enabling range and range-rate measurements collected between a satellite in the TDRSS constellation and a low-altitude satellite. In principle, a constellation of three satellites in equatorial, geosynchronous orbit separated by 120 degrees can provide continuous tracking coverage of low Earth orbiters. In addition to the satellite constellation, a ground station provides the crucial link back to the ground.

The basic TDRSS constellation consists of two operational satellites with an angular separation of 130°, which provides 85%–100% coverage for low-altitude satellites. For redundancy, on-orbit satellite spares are included in the constellation. Most of the operational satellites and stored spares are clustered near 41° W and 171° W, with one satellite at 275° W. The system is supported by a ground complex located at White Sands, New Mexico, with a remote extension in Guam. The constellation consisted of eight satellites in mid-2002, including some of the original satellites and two of a new generation of satellites, known as TDRS-H, -I, and -J in the prelaunch naming convention. TDRS-H was launched on June 30, 2000, and it was renamed TDRS-8 when it was accepted in October, 2001. The position of TDRS-8 is 171° W. TDRS-I and -J were launched in 2002 and were stationed at 150° W and 150.7° W.

With the definitions applied previously, the TDRSS employs *multiway* measurements. For example, a signal is transmitted from the White Sands complex to a TDRS in the K-band with a ranging code. This signal is retransmitted at the TDRS to a user satellite on S-band or K-band and, in turn, retransmitted back to the TDRS, where it is transmitted back to White Sands. Although the signal travels multiple paths, the basic observation equation is given by Eq. (3.3.10) for two-way range. In the case of TDRSS, however, corrections to this equation are required to account for delays at the respective instrumentation for signal retransmital, or transponder delays. Furthermore, the problem of determining the orbit of a user satellite is now linked to the problem of determining the orbit of the TDRS satellite used in the transmission links. It is evident that any errors in the TDRS orbit will map into errors for the user satellite, but the TDRS orbit errors may be accommodated by estimating the TDRS orbit parameters as well as those

for the user satellite. For detailed discussion on orbit determination using TDRSS, see papers by Rowlands *et al.* (1997) , Marshall *et al.* (1996), and Visser and Ambrosius (1997).

3.5.3 DOPPLER SYSTEMS

One-Way

A classic example of this technique has been the Navy Navigation Satellite System (NNSS) or Transit, which consisted of a constellation of several satellites in polar orbit. The NNSS began operation in the 1960s with the purpose that the constellation was to support navigation of U.S. Navy submarines. Operations in support of Navy applications ceased in the 1990s with the operational use of GPS. Each satellite carried a beacon that broadcasted signals with two frequencies for ionosphere correction: 150 MHz and 400 MHz. As described in Section 3.3.2, the receiver measured the Doppler count over specified intervals of time (e.g., 3.8 sec), thereby providing a measure of the Doppler shift or range-rate as the basic measurement for the navigation process.

In the 1970s, another spaceborne beacon was used for geodetic applications. For example, the satellite GEOS-3 carried an SLR reflector and beacons that broadcast signals at 162 MHz and 324 MHz, as well as a single-frequency radar altimeter operating at 13.9 GHz.

The French space agency, Centre National d'Etudes Spatiales (CNES), operates a Doppler system that utilizes ground-based beacons. In this system, the less expensive beacons are placed on the ground and a single receiver is carried on the satellite. This system, known as *DORIS (Doppler Orbitography and Radio positioning Integrated by Satellite)*, was used for the first time on the French imaging satellite, SPOT, in the 1980s, but this application was followed by use on TOPEX/Poseidon (see Fig. 3.5.5) in the early 1990s. DORIS will be used on several satellites to be operated in the early years of the 21st century. DORIS uses two frequencies for ionosphere correction: 401.25 MHz and 2036.25 MHz. DORIS measurements are usually processed as range-rate and the precision is better than 0.5 mm/sec.

The GPS carrier phase is another form of Doppler, although it is typically converted into a range measurement for processing. The basic measurement is usually extracted from the instrumentation as an integer number of cycles, measured since some start time, plus the fractional part of a cycle. The accumulated phase from the start time, expressed by Eq. (3.3.23), usually is converted into a distance measurement by multiplying with the wavelength of the signal (Eq. (3.5.3)), but the phase measurement can be converted into Doppler as an alternate measurement.

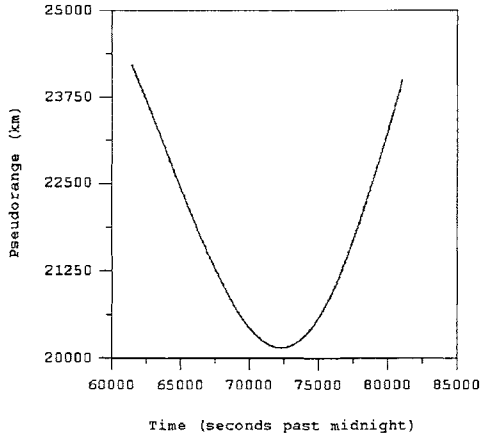

Figure 3.5.6: McDonald Observatory (MDO1) L1 pseudorange from PRN-6 on 19 June 1999. The uncorrected pseudorange as recorded by the receiver at a 30 second interval is shown. No pseudoranges were recorded for 200 seconds at about 67000 seconds.

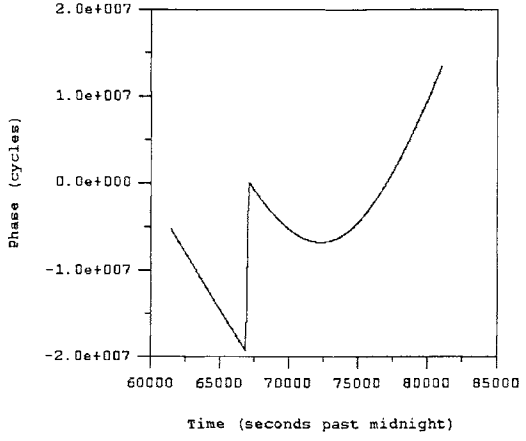

Figure 3.5.7: McDonald Observatory (MDO1) L1 carrier phase from PRN-6 on 19 June 1999. The uncorrected carrier phase as recorded by the receiver at a 30 second interval is shown. A 200 second interval where the receiver loses count of cycles is evident as the discontinuity.

3.5.4 EXAMPLES

GPS

Figures 3.5.6 and 3.5.7 illustrate measurements acquired by a GPS receiver (known as MDO1) at McDonald Observatory, near Ft. Davis, Texas. The receiver was a TurboRogue SNR8000 with a choke-ring antenna. The data were obtained on June 19, 1999, and recorded at a 30-second interval. Figure 3.5.6 shows the L1 pseudorange, expressed in kilometers, obtained from PRN-6. The measurements were recorded by the receiver at a 30-second interval. The SNR8000 receiver performs a *clock-steering*, meaning that the receiver reference oscillator is changed (a disciplined oscillator) so that the clock is steered toward GPS-Time, thereby closely synchronizing the receiver with GPS-Time to better than 100 ns. However, the MDO1 receiver uses an externally controlled high-quality quartz reference oscillator that is also used by the SLR system (known as *MLRS*), which is adjusted to GPS-Time separately.

The SNR8000 is an example of a class of geodetic quality receivers available from several vendors (e.g., Trimble Navigation, Ashtech, and Leica). These receivers simultaneously track the signals from up to 12 GPS satellites. The receiver used at MDO1 could track up to eight satellites. In spite of Y-code transmission (encrypted P-code) by the GPS satellites, the receivers provide measurements of pseudorange and carrier phase on L1 and L2 at a selected time interval.

The L1 pseudorange measurement for PRN-6 as recorded by the receiver is illustrated in Fig. 3.5.6, which simply illustrates the expected pattern. Comparing this figure to the simulated case in Fig. 3.2.2 shows the expected effect of the higher altitude GPS satellite on the magnitude of the range and the point of closest approach.

The L1 carrier phase measurement for PRN-6 is illustrated in Fig. 3.5.7, where the units are in cycles. Aside from the difference in units, the carrier phase exhibits similar characteristics to the pseudorange, except for the obvious discontinuity at 67000 seconds that does not appear in the pseudorange. This discontinuity results from an event that caused the receiver to lose lock on all GPS satellites for about 200 seconds and when tracking resumes, the carrier phase count was reinitialized to zero. On the other hand, since the pseudorange is based on code-correlation, there is no discontinuity. A discontinuity in carrier phase is referred to as *cycle slip*, which may produce dramatic discontinuities such as the Fig. 3.5.7 case, but they commonly produce cases where a small number of cycles are lost. Various techniques have been developed to fix cycle slips, which amount to using the carrier phase data before and after the discontinuity to estimate the integer number of cycles to adjust the data to create a continuous change in carrier phase. The data sampling of 30 seconds and the 200-second data gap make this particular cycle slip difficult to fix, but cases where the break may be a few cycles within the 30-second recording are straightforward to repair. If the cycle slip cannot be fixed,

Table 3.5.3:

ITRF-2000 Coordinates and Velocities for MDO1 and PIE1 Reference Points

ID	P/V	x	y	z
MDO1[1]	P	−1329998.6780	−5328393.3870	3236504.1990
	V	−0.0125	−0.0001	−0.0065
PIE1[2]	P	−1640916.7930	−5014781.2040	3575447.1420
	V	−0.0147	−0.0006	−0.0084

[1]Location: McDonald Observatory, Texas
[2]Location: Pie Town, New Mexico

Position (P) for January 1, 1997, in meters; velocity (V) in meters per year. The station velocity is caused primarily by tectonic plate motion. Since both stations are fixed to the North American Plate, which is rotating as a rigid plate, their velocities are similar. (xyz) is the ECF realized by ITRF-2000.

the single pass may be divided into two passes where the pass division occurs at the break.

The L_1 carrier phase can be converted to phase-range, a form of pseudorange, by multiplying by the signal wavelength (19 cm). This form of the range is given in Eq. (3.3.23), where the linear term disappears when f_G equals f_T, which is the case for this receiver. Direct comparison of the phase-range to the pseudorange derived from the transmitted code (Figs. 3.5.6 and 3.5.7) shows that there is a large bias between the two forms of pseudorange. This bias is caused by an *ambiguity* in the phase measurement (the term $\widetilde{N}$ in Eq. (3.5.2)), which results from the lack of any unique feature in individual cycles that can be correlated with time. In the pseudorange measurement based on a code, the correlation with time is performed because of the unique character of the code sequence. With carrier phase measurements, various techniques have been developed for *ambiguity resolution*; that is, determination of $\widetilde{N}$. Such techniques are attractive since the precision of phase-range is a few millimeters, whereas code pseudorange is decimeter-level. By resolving the ambiguity in the carrier phase measurement, the phase-range is significantly more precise than code pseudorange.

The quality of the measurements cannot be ascertained from Figs. 3.5.6 and 3.5.7, since the character is dominated by the orbital motion. For this example, the orbit position will be assumed to be known, thereby allowing a computed range, C, to be obtained and the residual O-C to be generated. By removing the dominant orbital motion effect, the measurement quality (including the quality of

Table 3.5.4:
Contributing Errors to Figs. 3.5.8 and 3.5.9

(O-C) Contributing Errors	Expected Error Magnitude
Use of geometric range	$\sim$ 100m
Satellite and receiver clock corrections	$\sim$ 100m
Selective Availability (SA)	$\sim$ 50m
Ionosphere and troposphere corrections	$\sim$ 10m
Transmit phase center	$<$ 1m
Receiver phase center	$<$ 0.1m
Receiver noise	0.5m
IGS ephemeris and ITRF coordinates	0.1m

the computed range) can be more readily exhibited.

Using the IGS final ephemeris and ECF coordinates of the receiver, the O-C can be computed for both code pseudorange and phase-range. For the cases described in the following paragraphs, the ITRF-2000 coordinates for the MDO1 site are given in Table 3.5.3. The time tag of each measurement recorded by this receiver is the *receive time* and the IGS ephemeris for the satellite is provided at an interval of 15 min. The MDO1 coordinates refer to the location of a specific reference point expressed with respect to the Earth center of mass as implied by the use of ITRF-2000. The IGS ephemeris for the PRN-6 center of mass actually refers to ITRF-97, but the difference between ITRF-97 and ITRF-2000 ephemerides is small.

The residual O-C for MDO1 is shown in Fig. 3.5.8, after removal of the computed range from the recorded pseudorange shown in Fig. 3.5.6. For this example, the computed range, C, was formed in the ECF using Eq. (3.2.4), with no corrections applied. Since no corrections have been made and geometric range was used for C, the error sources contributing to these residuals are summarized in Table 3.5.4.

When the residuals are computed for an IGS receiver located at Pie Town, New Mexico (known as PIE1 and located about 550 km northwest of MDO1), strong similarities are observed. Figure 3.5.9 shows the PIE1 residuals, with the computed range formed under the same assumptions as those for MDO1 in Fig. 3.5.8. Both Figs. 3.5.8 and 3.5.9 are dominated by two characteristics: an average linear trend and periodic variations. Close inspection of the periodic variations

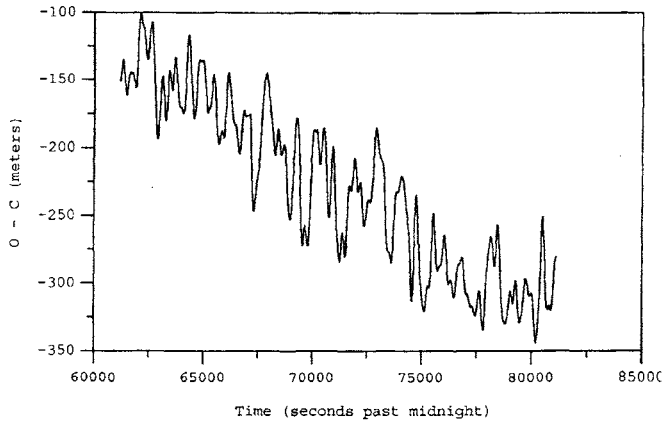

Figure 3.5.8: MDO1 L_1 pseudorange residuals (O-C) from 19 June 1998 for PRN6. The computed pseudorange (C) was obtained from the geometric range at signal receive time with no corrections. The one meter measurement noise is not evident at this scale since the O-C characteristics are dominated by an overall drift and high-frequency variations.

shows that this effect is essentially identical at both receivers. Using terminology introduced later in this book, one would say that the two characteristics have a high *correlation*. Of the sources listed in Table 3.5.4, only *Selective Availability* (SA) is expected to exhibit the somewhat periodic variations shown. In fact, repeating the same experiment one year later after SA has been "turned off" shows no evidence of these variations. The direct removal of SA is limited by the fact that information about the SA characteristics is classified, which eliminates the direct removal for nonclassified applications. The usual alternate approach, which is described in a later section, is to difference Figs. 3.5.8 and 3.5.9, which removes errors that are common to both receivers, such as SA.

After SA, the next dominant characteristics in the residuals are the nonzero mean and the linear slope that remains after "removal" of the mean and the periodic variations. Both the nonzero mean and the linear slope are caused by uncorrected clock errors, with some contribution from the generation of the computed range using the geometric range.

With the expectation that the receiver coordinates and the IGS ephemerides for the GPS satellites have errors at the decimeter level (see Table 3.5.4), the plots for (O-C) would show only random noise at the 50-cm level if the one-way range were properly computed from the available information, the clock errors were corrected, and the atmospheric delays were accounted for. The two receivers used

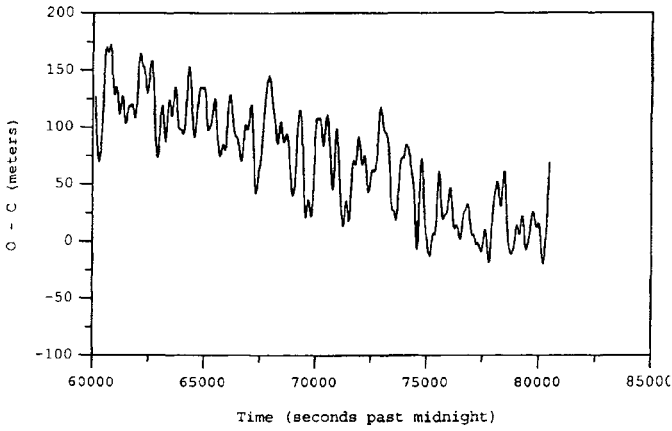

Figure 3.5.9: PIE1 $L - 1$ pseudorange residuals (O-C) for PRN6 from 19 June 1998. These residuals were formed with the same procedure used in Fig. 3.5.8. The high-frequency variations have a high correlation with those observed for the same time period at MDO1; therefore, these variations are not produced by the receiver. The variations are associated with Selective Availability.

in this example record pseudorange and carrier phase at a 30-second interval.

If carrier phase is converted to range, the plots for (O-C) would be dominated by a very large bias: the phase ambiguity term. However, removal of the ambiguity results in residual plots with characteristics very similar to Figs. 3.5.8 and 3.5.9. Since phase-range noise is usually a few millimeters, removal of the effects described in the preceding paragraph would illustrate the low noise level. The instrument noise statistics are usually used to describe the *measurement precision.*

DORIS

An example of DORIS measurements obtained from TOPEX/Poseidon is shown in Fig. 3.5.10. The data in this figure are based on a DORIS beacon located at Fairbanks, Alaska. Both DORIS frequencies were used to remove the ionosphere, but there would be no noticeable difference on the scale shown if the plot had been made using a single-frequency measurement.

Altimeter

As previously described, the altimeter measurement is based on two-way time of flight. The altimeter antenna is directed toward the nadir and a one-way range

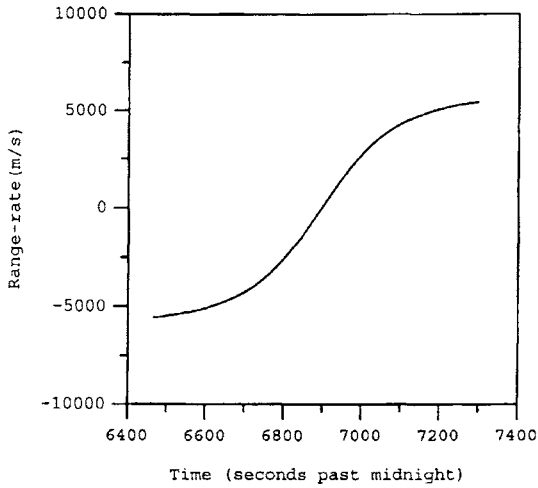

Figure 3.5.10: DORIS Range-rate from TOPEX/Poseidon on June 8, 1999.

(altitude) is formed by dividing the round-trip time-of-flight by two. The TOPEX altimeter data collected during a long pass over the Pacific (TOPEX/Poseidon Repeat Cycle 303) are shown in Fig. 3.5.11. For this example, the dual-frequency correction for the ionosphere was made, along with other corrections, at the meter level. The T/P orbit is frozen (see Chapter 2) with argument of perigee at 90°, which occurs just past 35500 seconds. As illustrated, the minimum altitude occurs near 34500 seconds, approximately corresponding to a latitude of 0°. The apparent contradiction of the perigee location and the minimum altitude is explained by the ellipsoidal character of the Earth, which plays a dominant role in Fig. 3.5.11, since the eccentricity of the T/P orbit is small (< 0.001).

Using an ephemeris of high accuracy for T/P, a computed altitude (C) to the Earth ellipsoid can be formed. The altitude residual, O-C, can be generated and is shown in Fig. 3.5.12, using satelllite geodetic latitude for the abscissa. The geodetic latitude at $-65.7°$ corresponds to the initial time of 32759 seconds. The residuals illustrate the profile of the ocean surface, expressed with respect to a reference ellipsoid, since this pass crosses mostly ocean.

3.6 DIFFERENCED MEASUREMENTS

In some cases, the measurements made by a particular technique are differenced in special ways. The differencing of the measurements removes or dimin-

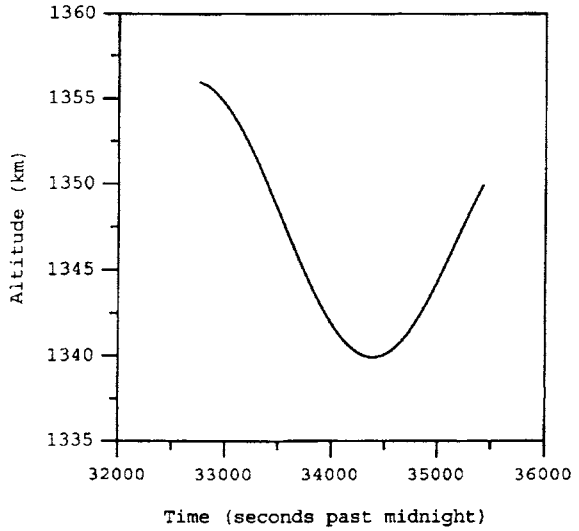

Figure 3.5.11: The TOPEX altimeter data collected during a long pass over the Pacific (TOPEX/Poseidon Repeat Cycle 303) are shown here.

ishes one or more error sources. The most common use of such differencing is with GPS pseudorange and carrier phase measurements and with altimeter measurements.

3.6.1 Differenced GPS Measurements

Figures 3.5.8 and 3.5.9 show a very clear correlation in high-frequency variations in the PRN-6 pseudorange residuals collected with two receivers separated by 550 km, as discussed in Section 3.5.4. These variations are caused by *Selective Availability* (SA), an intentional dithering of the broadcasting satellite clock. SA was turned off in May 2000, but provides an excellent example of the application of differenced data. An obvious approach to removing this effect is to difference the residuals (or the measurements) shown in Figs. 3.5.8 and 3.5.9, which is referred to as a *single difference (SD)*. In this case, the pseudorange measurements (or carrier phase) from a specific GPS satellite recorded at two different receivers can be differenced to produce:

$$SD^i_{jk} = \rho^i_j - \rho^i_k \tag{3.6.1}$$

where i identifies the GPS satellite, j identifies one receiver, and k identifies the other receiver. Alternatively, the single difference could be formed using mea-

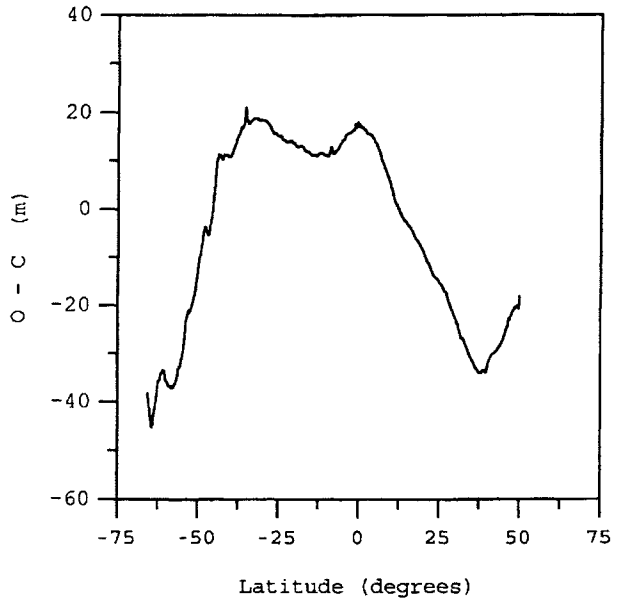

Figure 3.5.12: The geodetic altitude residual, O-C, can be illustrated using satellite geodetic latitude for the abscissa, as shown here. The O-C is generated from the observed geodetic altitude (Fig. 3.5.11) and a computed altitude formed from a TOPEX ephemeris determined form DORIS and SLR. The residual illustrates the along-track ocean surface profile with respect to the reference ellipsoid.

surements collected by one receiver and two different satellites.

An SD residual can be formed from the *a priori* receiver coordinates and the given coordinates for the broadcasting satellites to generate the *computed SD*. Hence, the SD residual is

$$SD(O-C)^i_{jk} = (O-C)^i_j - (O-C)^i_k, \tag{3.6.2}$$

where O can be either pseudorange or carrier phase and SD$(O-C)$ represents the single difference residual using satellite i and receivers j and k. Using Eq. (3.6.2), if the residuals shown in Fig. 3.5.8 are differenced with those in Fig. 3.5.9, the result is shown in Fig. 3.6.1, where it is evident that the SA high-frequency variations have been removed.

The single-difference residuals formed using a different satellite, PRN-30, are shown in Fig. 3.6.2. Although they are not shown, the residuals formed in the same way as Fig. 3.5.8 or 3.5.9, but using PRN-30 instead of PRN-6, exhibit similar high-frequency variations. Since the SA effect is satellite-dependent, the

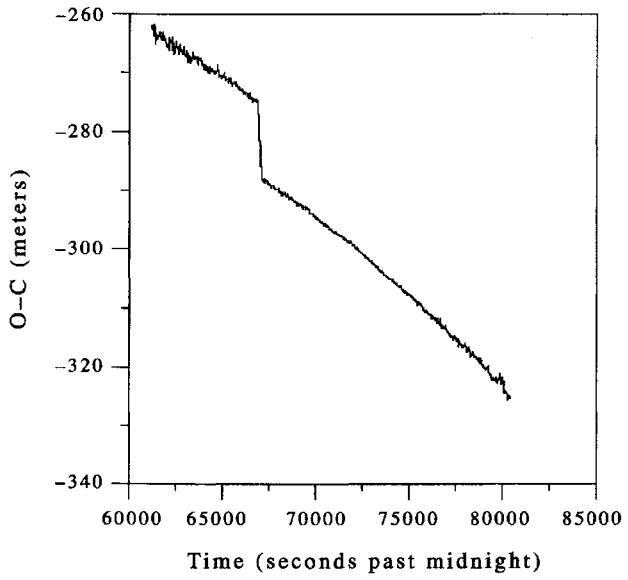

Figure 3.6.1: Single difference L1 pseudorange residuals formed with PRN-6, MDO1, and PIE1.

difference in the specific characteristics of the high-frequency variations is expected.

The SD behavior shown in Figs. 3.6.1 and 3.6.2 warrants further discussion. The formation of the SD has removed most of the high-frequency variations that are evident in Figs. 3.5.8 and 3.5.9. The remaining SD residuals exhibit a linear slope, a discontinuity at about 67000 sec, and some very small amplitude variations with an apparent high frequency. The remaining linear slope suggests that the effect is caused by sources that are not common in the data collected by the two receivers. Such effects include errors in the respective receiver clocks, errors contributed by atmosphere delays, and errors in the approximation of the computed range by the geometric range. Although the receiver separation of 550 km perhaps seems large, it is not when compared to the GPS orbit radius of 26000 km. Since both PRN-6 and PRN-30 are within view of each receiver, the line-of-sight to each satellite from the respective receiver is similar, which means that the atmospheric delays will be very similar and some portion (but not all) of the atmospheric delay will be removed in the SD formation. Errors associated with use of geometric range will partially cancel in the SD as well. However, the clock

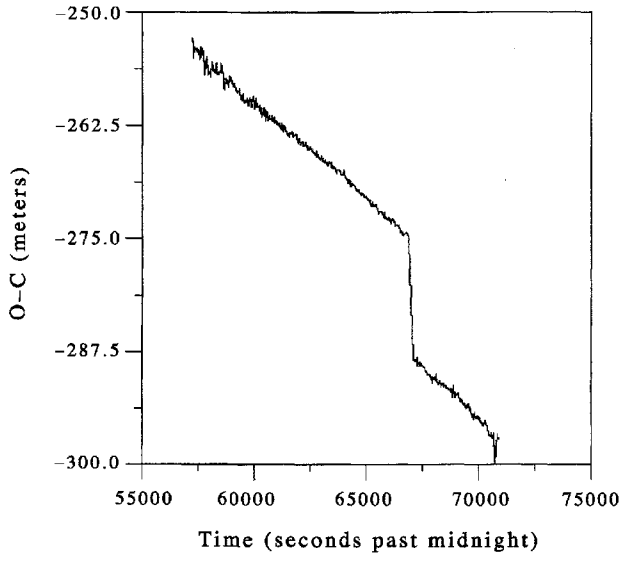

Figure 3.6.2: Single difference L1 pseudorange residuals formed with PRN-30, MDO1, and PIE1.

behavior of each receiver will be different and cannot be expected to cancel. As a consequence, receiver clock errors are expected to be the dominant error source that produces the linear variation in SD residuals shown in Figs. 3.6.1 and 3.6.2.

The discontinuity in Figs. 3.6.1 and 3.6.2 is another matter. This discontinuity occurs when the MDO1 receiver did not record data, but the PIE1 receiver does not show a gap in the data record. Although the precise cause of the discontinuity is not known, it appears to be associated with some event at MDO1, such as a clock anomaly related to the data gap.

The third characteristic evident in the SD residuals is an apparently small amplitude variation, which exhibits larger amplitude at the endpoints. These endpoints correlate with satellite rise and satellite set of one or both satellites. Clearly, SD measurements require that data from two satellites be available, so the difference between satellites requires that both satellites are located above the receiver horizon. The nature of these apparent high-frequency variations will become clearer in the following discussion.

The single differences for PRN-6 and PRN-30 can be further differenced to remove additional common errors. The resulting double difference (DD) is

$$DD_{jk}^{im} = SD_j^i - SD_k^m \tag{3.6.3}$$

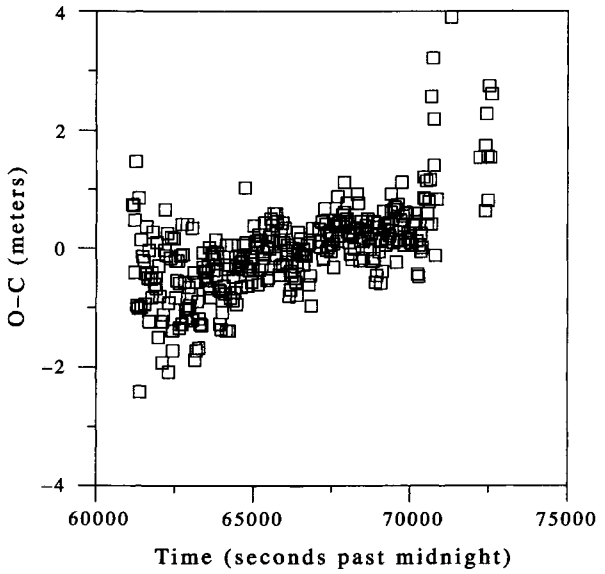

Figure 3.6.3: Double difference L1 pseudorange residuals formed from PRN-6, PRN-30, MDO1, and PIE1.

where DD represents the DD residual, formed between satellites i and m, and receivers j and k. The DD residual can be formed by differencing the single difference residuals, for example.

Double difference residuals can be formed by differencing the data used to create the plots of Figs. 3.6.1 and 3.6.2. The corresponding pseudorange DD residuals are shown in Fig. 3.6.4. It is evident that the dominant characteristics observed in the SD residuals have disappeared and the residuals are now scattered near zero. These residuals now exhibit a more random character and the only systematic characteristic is a slight linear slope. The fact that the Fig. 3.6.4 residuals are near zero demonstrates that the coordinates of the receivers given in Table 3.5.3 and the IGS ephemerides are quite accurate. If the receiver coordinates or the satellite ephemerides contained significant errors, the resulting DD residuals would reflect those errors, though not necessarily in a one-to-one ratio.

Note these additional points from Fig. 3.6.4. The obvious scatter is referred to as a *measurement noise* or *measurement precision.* The scatter seems to increase near the initial times and the final times, which is likely caused by low elevation effects at one or both receivers where the signal-to-noise ratio is degraded.

If the SD residuals had been computed using carrier phase (converted to phase

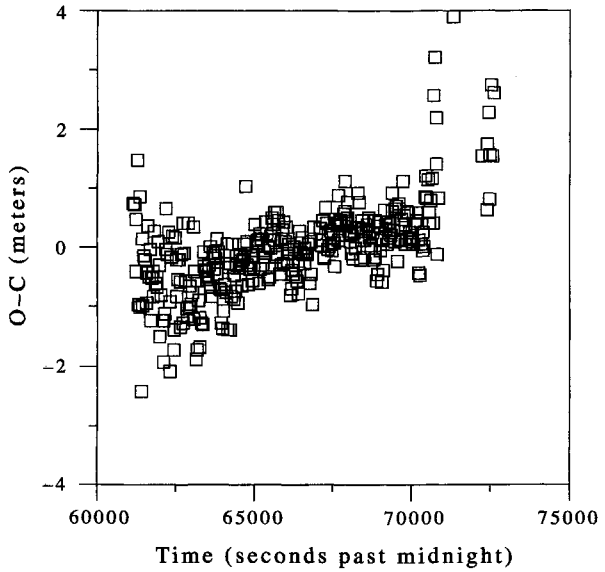

Figure 3.6.4: Double difference L1 pseudorange residuals formed from PRN-6, PRN-30, MDO1, and PIE1.

range) and if the computations had been performed in the same way as those for pseudorange described earlier, the residuals would have a large bias caused by the phase ambiguity. Without any correction for this ambiguity, the ambiguities in each of the phase range measurements would combine to produce a constant bias in the phase range DD residuals. Determination of the respective phase ambiguities is referred to as ambiguity resolution. In many cases the ambiguity may be estimated with other parameters in the estimation process. Once the phase ambiguity has been removed, either in the individual receiver/satellite measurements or as a combined term in the DD, the residuals formed after ambiguity removal would exhibit characteristics similar to Fig. 3.6.4, with the major exception that the residuals would be at the level of a few millimeters instead of the meter level evident in Fig. 3.6.4.

3.6.2 Differenced Altimeter Data

Although a satellite-borne altimeter has a distinct advantage in its global distribution of data, consideration of possible error sources when altimeter data are directly used for orbit determination suggests several disadvantages. In particu-

lar, long wavelength oceanographic features and nontemporal ocean topography can be absorbed into the orbit when altimeter data are directly used for orbit and geodetic parameter determination. The nontemporal ocean topography, mostly due to error in the global geoid, has meter-level uncertainty and is significant when decimeter radial orbit accuracy of certain satellites, such as TOPEX/Poseidon, is desired.

A technique that eliminates the altimeter dependence on the nontemporal ocean topography is the use of altimeter measurements at the points where the orbit ground track intersects. These points are referred to as *crossover points*, and the differenced altimeter measurements at these points are referred to as *crossover measurements*.

Crossovers have been valuable for the evaluation of radial orbit ephemeris error. Although the nontemporal portion of the ocean topography can be eliminated at the crossover point, the remaining temporal changes, such as ocean tide, unmodeled orbit error, short wavelength phenomena, as well as altimeter time tag error, can still be aliased into the radial orbit error on a global basis. With the exception of the geographically correlated error due to inaccuracy in the Earth's gravity field (Christensen *et al.*, 1994) , global computation and analysis of crossover residuals can provide valuable information about radial orbit error sources.

In order to use crossover measurements, several procedures that are unique to these measurements must be employed. First the crossover times, t_i and t_j, must be generated from a nominal orbit. This nominal orbit may have been previously determined from a least squares estimate using GPS data or ground-based tracking data such as laser range. The crossover times t_i and t_j are computed using a ground track corresponding to the nominal orbit. The final results of this step are t_i and t_j for all crossover points in the nominal ephemeris.

The crossover measurements are generated using the crossover times. Since the altimeter measurements are usually recorded at a fixed time interval, it is rare that a measurement will exactly correspond to the crossover times (t_i and t_j). As a consequence, the altimeter measurements in the vicinity of each crossover time are used to create a pseudo-measurement, by the application of an interpolating function evaluated at the crossover time. Candidate interpolating functions include a least squares cubic spline, but other functions may be used. Depending on the nature of the surface (such as laser altimeter data on rough land surfaces), which may produce altimeter data with more noise than on a smooth surface, care must be taken in the application of an interpolating function to minimize the effect of the noise. With pseduo-measurements at each crossover time, the crossover measurement is obtained by differencing the two measurements and the crossover is assigned two time tags, t_i and t_j. For most applications, the crossovers should be formed consistently, such as the ascending track pseudo-measurement minus the descending track pseudo-measurement. To facilitate subsequent application in

the estimation process, these crossover measurements may be sorted in chronological order of the ascending track time. Additional information on altimeter crossover measurements can be found in Born *et al.* (1986) , Shum *et al.* (1990), and Lemoine *et al.* (2001).

3.7 SATELLITE POSITIONS

In some cases, the observational set may be an ephemeris of satellite positions. The estimation techniques of the following chapters can be applied to such observations. Depending on the source of the ephemeris, it may exhibit a variety of error sources that depend on the methodology used to derive the ephemeris.

A commonly used ephemeris can be readily obtained if the satellite carries a GPS receiver. The GPS receiver usually provides its position in near real time from pseudorange measurements and the ephemeris information broadcast by the GPS satellites. As described in Section 3.5.1, a GPS receiver extracts the broadcast ephemeris and clock parameters from the information superimposed on the carrier signal. Equation (3.5.1) gives the relationship for pseudorange as

$$\tilde{\rho} = \rho + c(\delta t_R - \delta t_T) + \delta\rho_{\text{trop}} + \delta\rho_{\text{ion}} + \epsilon.$$

With a receiver carried on a LEO satellite, the GPS signals arriving at the antenna do not pass through the troposphere unless the antenna is oriented at a significant angle with respect to the zenith direction, so the term $\delta\rho_{\text{trop}}$ usually can be ignored. The ionosphere contribution, $\delta\rho_{\text{ion}}$, may be small at LEO satellite altitude (e.g., < 10 cm at TOPEX altitude). As a consequence, the term can be ignored for some applications, but it is required for the most demanding applications with high accuracy. For those applications where the ionosphere term is required, some GPS receiver provides two frequency measurements and the correction for the ionosphere can readily be made with Eq. (3.4.14). Another approach is to apply a model for the ionosphere if a single-frequency receiver is available, but the accuracy of the correction will be degraded with respect to the dual-frequency measurement.

The transmitter clock correction in Eq. (3.5.1), δt_T, can be determined from the set of parameters broadcast by the satellite (or from other sources) for its clock and ρ is dependent on the GPS satellite position at the transmit time and the receiver position at the receive time. In the preceding equation, the unknowns are the receiver clock correction (δt_R) and the position vector of the GPS receiver carried on a LEO, which defines four unknowns. If the receiver measures the pseudorange from a minimum of four or more GPS satellites, then four equations similar to the preceding equation can be formed for each of the observed GPS satellite, which defines a system of four nonlinear algebraic equations. If more than four GPS satellites are visible, then an overdetermined system of equations

exists. Such a system of equations can be solved using, for example, the Newton Raphson method. This method is described and applied to the solution of an overdetermined system of least squares equations in Section 4.3.4.

The solution for receiver position and clock offset is referred to as the *navigation solution* and it is commonly computed in near real time by GPS receivers, especially those designed for use on LEO satellites. Depending on the characteristics of the receiver, the accuracy of the position in the absence of Selective Availability is about 10 meters, where the error in the solution is dominated by the error in the GPS broadcast ephemerides. Nevertheless, an ephemeris formed by the navigation solution could be used as a set of observations in the application of an estimation algorithm (e.g., Thompson *et al.*, 2002).

The navigation solution is one form of *kinematic solution.* As the term implies, the solution is not dependent on the dynamical description of the satellite and the equations of motion (Eq. 2.3.46) are not required. A significant advantage for some applications is the fact that this solution can be generated in near real time. Another form of kinematic solution makes use of carrier phase measurements and the resolution of ambiguities to obtain a more accurate solution (Hofmann-Wellenhof *et al.*, 1997), but these solutions typically make use of high-accuracy GPS ephemerides, which usually preclude real-time LEO applications.

3.8 ANGLES

At the beginning of the space age, tracking of artificial satellites included an extension of astronomical techniques based on the use of photographic plates. With a camera mounted on a telescope, a photographic plate was produced for a region of the sky during a specified exposure time. Since the mount would compensate for the rotation of the Earth, stars would appear as dots but celestial bodies and artificial satellites would produce a streak on the plate since they move at non-sidereal rates. The Baker-Nunn system was introduced to track satellites using photographic techniques. In the modern era, the photographic plates have been replaced by a *Charge Coupled Device* (CCD) camera, but the methodology remains much the same. Calibration of the camera/mount is an important part of the operation of these instruments.

A photograph of a satellite streak against a background of stars provides a set of observations that can be deduced from the location of the satellite with respect to the nearby stars. The stellar coordinates can be determined from a star catalog, such as the catalog derived from the European Space Agency Hipparcos astrometry satellite. The basic set of satellite observations derived from the stellar coordinates are right ascension and declination, typically expressed with respect to J2000. One modern application of right ascension and declination observations

of a satellite is in space surveillance applications. For example, the *Air Force Maui Optical and Supercomputing* (AMOS) site operates several telescopes on Mt. Haleakala to support surveillance.

The remainder of the Minitrack system built to track the Vanguard satellites is now confined to the continental U.S., but this space fence (operated by the U.S. Navy to support space surveillance) provides angular measurements in terms of direction cosines. The space fence consists of a network of transmitters and receivers located along a great circle. When a satellite (including space debris) crosses the electronic fence, a set of measurements given by time and direction cosines are determined, which is introduced into a process to determine both the orbit of the object and its identity.

3.9 REFERENCES

Ashby, N., "Relativity and the Global Positioning System," *Physics Today*, Vol. 55, No. 5, pp. 41–47, May 2002.

Born, G. H., B. D. Tapley, and M. L. Santee, "Orbit determination using dual crossing arc altimetry," *Acta Astronautica*, Vol. 13, No. 4, pp. 157–163, 1986.

Christensen, E., B. Haines, K. C. McColl, and R. S. Nerem, "Observations of geographically correlated orbit errors for TOPEX/Poseidon using the Global Positioning System," *Geophys. Res. Ltrs.*, Vol. 21, No. 19, pp. 2175–2178, Sept. 15, 1994.

Degnan, J., and J. McGarry, "SLR2000: Eyesafe and autonomous satellite laser ranging at kilohertz rates," *SPIE Vol. 3218, Laser Radar Ranging and Atmospheric Lidar Techniques*, pp. 63–77, London, 1997.

Dunn, C., W. Bertiger, Y. Bar-Sever, S. Desai, B. Haines, D. Kuang, G. Franklin, I. Harris, G. Kruizinga, T. Meehan, S. Nandi, D. Nguyen, T. Rogstad, J. Thomas, J. Tien, L. Romans, M. Watkins, S. C. Wu, S. Bettadpur, and J. Kim, "Instrument of GRACE," *GPS World*, Vol. 14, No. 2, pp. 16–28, February 2003.

Herring, T., "Modeling atmospheric delays in the analysis of space geodetic data," in *Refraction of Transatmospheric Signals in Geodesy*, J. C. DeMunck and T. A. Th. Spoelstra (eds.), Netherlands Geodetic Commission Publications in Geodesy, 36, pp. 157–164, 1992.

Hofmann-Wellenhof, B., H. Lichtenegger, and J. Collins, *Global Positioning System: Theory and Practice*, Springer-Verlag, Wien-New York, 1997.

Leick, A., *GPS Satellite Surveying*, J. Wiley & Sons, Inc., New York, 2003.

Lemoine, F., D. Rowlands, S. Luthcke, N. Zelensky, D. Chinn, D. Pavlis, and G. Marr, "Precise orbit determination of GEOSAT follow-on using satellite laser ranging and intermission altimeter crossovers," NASA/CP-2001-209986, *Flight Mechanics Symposium*, John Lynch (ed.), NASA Goddard Space Flight Center, Greenbelt, MD, pp. 377–392, June 2001.

Marini, J. W., and C. W. Murray, "Correction of laser range tracking data for atmospheric refraction at elevations above 10 degrees," *NASA GSFC X591-73-351*, Greenbelt, MD, 1973.

Marshall, J. A., F. J. Lerch, S. B. Luthcke, R. G. Williamson, and C. Chan, "An Assessment of TDRSS for Precision Orbit Determination," *J. Astronaut. Sci.*, Vol. 44, No. 1, pp. 115–127, January–March, 1996.

Montenbruck, O., and E. Gill, *Satellite Orbits: Models, Methods, and Applications*, Springer-Verlag, Berlin, 2001.

Parkinson, B., J. Spilker, P. Axelrad, and P. Enge (eds.), *Global Positioning System: Theory and Applications*, Vols. 1–3, American Institute of Aeronautics and Astronautics, Inc., Washington DC, 1966.

Ries, J. C., C. Huang, M. M. Watkins, and B. D. Tapley, "Orbit determination in the relativistic geocentric reference frame," *J. Astronaut. Sci.*, Vol. 39, No. 2, pp. 173–181, April–June 1991.

Rowlands, D. D., S. B. Luthcke, J. A. Marshall, C. M. Cox, R. G. Williamson, and S. C. Rowton, "Space Shuttle precision orbit determination in support of SLA-1 using TDRSS and GPS tracking data," *J. Astronaut. Sci.*, Vol. 45, No. 1, pp. 113–129, January–March 1997.

Saastamoinen, J., "Atmospheric correction for the troposphere and stratosphere in radio ranging of satellites," *Geophysical Monograph Series, Vol. 15*, S. Henriksen, A. Mancini, B. Chovitz (eds.), American Geophysical Union, Washington, DC, pp. 247–251, 1972.

Seeber, G., *Satellite Geodesy: Foundations, Methods & Applications*, Walter de Gruyter, New York, 1993.

Shum, C. K., B. Zhang, B. Schutz, and B. Tapley, "Altimeter crossover methods for precise orbit determination and the mapping of geophysical parameters," *J. Astronaut. Sci.*, Vol. 38, No. 3, pp. 355–368, July–September 1990.

Skolnik, M.I. (ed.), *Radar Handbook*, McGraw-Hill, New York, 1990.

Thompson, B., M. Meek, K. Gold, P. Axelrad, G. Born, and D. Kubitschek, "Orbit determination for the QUIKSCAT spacecraft," *J. Spacecr. Rockets*, Vol. 39, No. 6, pp. 852–858, November–December 2002.

Visser, P., and B. Ambrosius, "Orbit determination of TOPEX/Poseidon and TDRSS satellites using TDRSS and BRTS tracking," *Adv. Space Res.*, Vol. 19, pp. 1641–1644, 1997.

Wells, D., *Guide GPS Positioning*, Canadian GPS Associates, Fredericton, 1987.

3.10 EXERCISES

1. Determine the Doppler shift in frequency over a pass for:

   a. TRANSIT: 150 MHz

   b. GPS: 1575 MHz

   To simplify this problem, assume the satellite is in a posigrade equatorial orbit and the observer is located on the equator. Determine the Doppler shift when the satellite rises and sets on the observer's local horizon and when the satellite is at closest approach to the observer.

2. The TOPEX/Poseidon spacecraft, launched in August 1992, carried a GPS receiver. At the following date and time, the receiver made the following measurements:

   Date/time: 31 March 1993 02:00:00.000 (receiver time)

GPS PRN	L1 pseudorange (m)
21	−16049870.249
28	−14818339.994

   From other sources, the T/P position at this time was determined to be

x	−2107527.21m
y	6247884.75
z	−4010524.01

   where (x, y, z) is ECF. The positions of the GPS satellites at this time were

	PRN21	PRN28
x	10800116.93m	10414902.30
y	23914912.70	13538107.48
z	1934886.67	−20329185.40

where these positions are expressed in the same reference frame as T/P.

Determine the T/P GPS receiver clock offset using both satellites. Ignore the GPS transmitter clock correction. State and justify any assumptions.

3. Repeat the example in Section 3.3.1 but use orbit altitudes of

   a. Lageos (5900 km)

   b. GPS (20,000 km)

   c. Moon (380,000 km)

The following data apply to Exercises 4–13:

GPS Ephemerides

The following ephemerides were taken from the "IGS final ephemerides" and the format is similar to the SP-3 format used by IGS:

*YR/MO/DA HR:MN:SEC					
P	PRN	x	y	z	δt_T
	⋮				
P	PRN	x	y	z	δt_T

where time is given in GPS-Time as

YR = Year

MO = Month of year

DA = Day of month

HR = Hour of day

MN = Minutes

SEC = Seconds

The lines following the epoch line are

P = Position ephemeris

PRN = GPS Satellite identifier

x,y,z = ITRF-2000 position of GPS PRN, in km

δt_T = IGS-determined clock offset for PRN, in microseconds

* 2003/7/3 5:45:0.00000000					
P	1	4566.504088	−17778.663761	−19019.826900	292.783269
P	4	−10978.897783	−10863.301011	−21544.271426	44.796690
P	7	−16743.206878	−20415.491050	−3315.879862	556.798655
P	8	−4587.665320	−17960.987250	18706.552158	378.701406
P	11	14431.377269	−21405.604003	6070.147167	54.319645
P	13	−4652.983492	−23260.723995	−12070.391803	−29.105842
P	27	1214.284685	−23377.459743	12442.855885	377.394607
P	28	−14937.324209	−12545.945359	18318.739786	−28.452370
P	29	−17278.539907	−1224.933899	20384.228178	155.457984
P	31	13278.146508	−8114.211495	21225.174835	300.884498
* 2003/7/3 6:0:0.00000000					
P	1	5861.745350	−15901.667555	−20276.875963	292.785440
P	4	−9777.977569	−12987.742895	−20912.838681	44.796231
P	7	−16651.970525	−20805.209726	−525.893274	556.811719
P	8	−3449.706143	−19727.772705	17096.293643	378.709764
P	11	14464.812694	−20477.667957	8654.011503	54.321275
P	13	−3700.036312	−22089.587975	−14378.853276	−29.106054
P	27	1969.580616	−24408.106473	10001.540814	377.440654
P	28	−12810.474492	−12772.984277	19707.048914	−28.448653
P	29	−18461.999653	−3089.021101	19091.163769	155.460061
P	31	14725.051413	−6093.976687	20978.562271	300.903599
* 2003/7/3 6:15:0.00000000					
P	1	7328.259794	−13996.483360	−21179.722738	292.788770
P	4	−8727.133318	−15090.465960	−19918.643118	44.795835
P	7	−16383.736913	−20953.296813	2273.086980	556.824434
P	8	−2489.551621	−21368.525118	15184.136954	378.718629
P	11	14449.564065	−19284.658838	11088.302121	54.322742
P	13	−2536.235846	−20774.358288	−16441.402012	−29.106257
P	27	2578.663020	−25207.610015	7386.006812	377.487071
P	28	−10560.925449	−13127.209192	20763.433991	−28.445536
P	29	−19645.300961	−4758.653980	17476.041504	155.462272
P	31	16233.527710	−4186.595815	20362.080900	300.922651

Observations

The following data are given in a format that is similar to the Receiver INdependent EXchange (RINEX) format for GPS receiver observations (refer to IGS for RINEX details):

YR/MO/DA	HR:MN:SEC	EF	N	PRN-List
L1	L2	P2		P1
⋮				
L1	L2	P2		P1

where time is given in GPS receiver time (close to GPS-Time) and

YR = Year

MO = Month of year

DA = Day of month

HR = Hour of day

MN = Minutes

SEC = Seconds

EF = Epoch Flag (0 means no problem)

N = Number of tracked GPS satellites

PRN-List = list of PRN-identifiers of tracked GPS satellites

The lines following the epoch line contain the observations for the PRN satellites, given in the same order as the PRN-list. In the observations:

L1 = L1 carrier phase (cycles)

L2 = L2 carrier phase (cycles)

P2 = L2 pseudorange (meters)

P1 = L1 pseudorange (meters)

(Note that fourth and fifth digits to right of decimal for carrier phase pertain to signal strength.)

The following data were recorded by a Black Jack receiver carried on ICESat:

2003/7/3 6:0:0.0000000	0 8 1 4 7 8 11 13 27 28		
13313150.27606	10373859.94706	25276179.66000	25276168.63500
3638113.46106	2834889.84706	25214111.21600	25214104.18700
−8930705.47408	−6958991.53008	20768986.07800	20768979.92300
−6413864.84708	−4997816.68208	20025186.23300	20025180.71900
−10979121.08307	−8555158.14008	22308126.25500	22308121.45400
−2786774.49707	−2171514.86607	22773866.90400	22773861.60000
−23434105.64308	−18260340.20309	19833911.31900	19833905.82300
−7593037.70208	−5916651.79208	21846321.76500	21846317.42700
2003/7/3 6:0:10.0000000	0 8 1 4 7 8 11 13 27 28		
13739083.01006	10705752.39405	25357229.60300	25357220.91900
3975221.46206	3097571.22406	25278260.02000	25278253.89400
−8829945.83208	−6880477.50608	20788159.91600	20788153.76600
−6629467.22309	−5165818.45908	19984158.47600	19984153.00800
−10987968.90807	−8562052.48708	22306442.29400	22306437.67400
−2390872.85807	−1863020.13207	22849204.79500	22849199.34400
−23466816.37608	−18285829.03209	19827686.48700	19827681.02000
−7876627.23108	−6137630.55108	21792356.26200	21792351.82000
2003/7/3 6:4:0.0000000	0 8 7 8 11 13 27 28 29 31		
−5513215.18608	−4296011.91608	21419312.62400	21419306.89400
−9854402.24209	−7678754.03309	19370472.81400	19370467.60200
−10546995.52107	−8218436.17807	22390355.62500	22390351.48800
7267464.77706	5662956.04106	24687125.70900	24687120.66100
−22384357.99608	−17442354.31309	20033670.90000	20033665.56700
−13406848.48208	−10446892.85208	20739989.40200	20739985.24200
−4806438.03607	−3745274.75407	22815283.89300	22815278.35000
−1904315.82106	−1483881.67706	23910972.26500	23910967.00200
2003/7/3 6:4:10.0000000	0 8 7 8 11 13 27 28 29 31		
−5327807.74108	−4151538.49708	21454594.42700	21454588.71500
−10500588.28407	−8182274.62907	22399186.76600	22399182.59700
7703560.72106	6002770.96806	24770114.33000	24770107.20000
−22259480.22808	−17345046.90309	20057434.39800	20057428.92100
−13598356.03208	−10596119.48608	20703546.53400	20703542.38700
−5057074.29907	−3940575.68207	22767589.44100	22767583.83300
−2109142.85306	−1643487.08006	23871994.45100	23871989.67700

The following data were collected by a Turbo Rogue GPS receiver at Pie Town (NM):

2003/7/3 6:0:0.0000000	0 8 8 27 26 11 29 28 31 7		
−24388891.10649	−19004308.54347	19950321.918	19950319.447
−23612111.74249	−18399018.28147	20633681.740	20633678.842
−354035.84848	−275871.64045	23938856.683	23938853.490
−6053270.88448	−4716827.20645	22881055.819	22881053.542
−11945499.34248	−9308173.13145	22918548.923	22918545.380
−21453687.95449	−16717124.87047	21107802.248	21107800.600
12464204.51048	9712367.70644	23823735.311	23823729.233
−4481731.59449	−3492253.10746	22002748.155	22002743.741
2003/7/3 6:4:0.0000000	0 8 8 27 26 11 29 28 31 7		
−24416407.84949	−19025750.07047	19945085.523	19945082.850
−23327037.21349	−18176882.46347	20687929.760	20687926.774
−898114.97748	−699828.98244	23835323.854	23835317.574
−6258015.55248	−4876368.11345	22842093.804	22842091.419
−12296146.77548	−9581404.44246	22851822.101	22851818.825
−21614641.52349	−16842543.10147	21077173.381	21077172.008
13324935.88948	10383067.35145	23987526.176	23987521.928
−5099063.91549	−3973290.68546	21885273.341	21885269.023

The following data were collected by a Turbo Rogue GPS receiver at McDonald Observatory (TX):

2003/7/3 6:0:0.0000000	0 8 29 27 11 8 13 26 28 7		
−9944212.12448	−7748726.63345	23401416.592	23401412.281
−24875552.81149	−19383519.73947	20395733.147	20395730.434
−11346725.95449	−8841595.17445	22528013.534	22528011.897
−28075193.49449	−21876748.09447	19982685.387	19982683.005
−4164302.39448	—	—	24437530.876
−2296772.12848	—	—	24480165.844
−18590371.83649	−14485969.70246	21419438.945	21419437.517
−16001981.31449	−12469051.09846	21932274.397	21932270.319

2003/7/3 6:4:0.0000000	0 8 29 27 11 8 13 26 28 7		
−10328700.49948	−8048327.52545	23328248.166	23328245.981
−24679310.88249	−19230604.03647	20433076.681	20433074.090
−11480544.84549	−8945869.42745	22502548.387	22502546.906
−28204694.64049	−21977658.03247	19958042.069	19958039.765
−3297123.18548	—	—	24602548.472
−2850548.61348	−2221193.01544	24374788.863	24374785.477
−18774076.61449	−14629116.05246	21384480.700	21384479.692
−16569301.13749	−12911117.94346	21824316.532	21824312.371

4. Use the ICESat data for any of the given epochs to determine:
   a. ionosphere-free pseudoranges for each satellite
   b. ionosphere correction to the L1 pseudoranges
   c. convert carrier phase to "phase range"
   d. ionosphere-free phase ranges for all satellites
5. Use the ICESat data separated by 10 sec and by 4 min to determine:
   a. range change over the respective time interval from pseudorange and phase range
   b. an approximate value of phase range ambiguity for each observed GPS. satellite
6. a. Determine an ICESat position at 06:00:00.000000 (and any other relevant parameters). Provide justification for the solved for parameter set and identify the measurements used. Strive for highest accuracy. Use all observed satellites, but provide justification for any satellites that should be edited from the solution. Identify and justify assumptions.
   b. Provide the O-C for each of the satellites used in a.
   c. Determine the azimuth and elevation of each GPS satellite with respect to the ICESat local horizontal plane and vertical direction using true north as a reference direction.
7. Repeat Exercise 6, but use the epoch 06:04:00.000000.
8. a. Form pseudorange single differences with the ICESat data at 06:00:00.000000. Identify the measurements used and strive for highest accuracy. Identify and justify assumptions.

b. Determine an ICESat position and any other relevant parameters using the single differences of a. Provide justification for the solved for parameter set.

c. Provide the O-C for all measurements used in b.

9. Repeat Exercise 8, but use the epoch 06:04:00.000000.

10. a. Form pseudorange double-difference measurements between ICESat and Pie Town at 06:00:00.000000. The coordinates for Pie Town and McDonald are given in Table 3.5.3.

b. Determine an ICESat position and any other relevant parameters using double differences of a. Provide justification for the solved for parameter set. Are the double differences in your solution independent (see Hoffman-Wellenhof *et al.*, 1997)? Strive for high accuracy. Identify and justify assumptions.

c. Provide the O-C for all measurements used in b.

11. Repeat Exercise 10, but use the epoch 06:04:00.000000.

12. Repeat Exercise 10, but use McDonald instead of Pie Town. State any assumptions.

13. Form double-difference pseudorange measurements between Pie Town and McDonald and compute the O-C using the available ephemerides and information from Table 3.5.3.